A continuous-discontinuous approach to simulate fracture processes in quasi-brittle materials

Peter Moonen, Jan Carmeliet, Bert Sluys

A continuous-discontinuous approach to simulate fracture processes in quasi-brittle materials

Journal:	*Philosophical Magazine & Philosophical Magazine Letters*
Manuscript ID:	TPHM-08-Jul-0261.R1
Journal Selection:	Philosophical Magazine
Date Submitted by the Author:	29-Sep-2008
Complete List of Authors:	Moonen, Peter; T.U. Delft, Department of Civil Engineering and Geosciences; K.U. Leuven, Department of Civil Engineering Carmeliet, Jan; Swiss Federal Laboratories for Materials Testing and Research (EMPA), Laboratory for Building Technologies; Swiss Federal Institute of Technology Zürich (ETH), Department of Architecture, Instutute for Building Technology Sluys, Bert; T.U. Delft, Department of Civil Engineering and Geosciences
Keywords:	fracture, mechanical behaviour
Keywords (user supplied):	X-FEM, continuous-discontinuous framework

A continuous-discontinuous approach to simulate fracture processes in quasi-brittle materials

P. Moonen[(1,2)], J. Carmeliet[(3,4)], L.J. Sluys[(1)]

(1) Department of Civil Engineering and Geosciences, Delft University of Technology, Stevinweg 1, 2628 CN Delft, The Netherlands
(2) Laboratory of Building Physics, Department of Civil Engineering, Katholieke Universiteit Leuven, Kasteelpark Arenberg 40, 3001 Leuven, Belgium
(3) Institute for Building Technology, Department of Architecture, Swiss Federal Institute of Technology Zürich (ETH), Wolfgang-Pauli-Str. 15, 8093 Zürich, Switzerland
(4) Laboratory for Building Technologies, Swiss Federal Laboratories for Materials Testing and Research (EMPA), Überlandstrasse 129, 8600 Dübendorf, Switzerland

1 Abstract

A macroscopic framework for the simulation of failure processes in quasi-brittle materials is proposed. The framework employs the partition of unity (PU) concept and introduces a new cohesive zone model, capturing the transition between the initial continuum state and the final discrete state. The model is generic in a sense that it allows extending most continuum models to a discontinuous framework in an efficient and robust way, hereby adding the effect of macro-crack formation by the growth and coalescence of micro-defects. Both material failure and interface failure can be studied with this formulation.

Keywords: fracture, cohesive zone model, X-FEM, continuous-discontinuous framework.

2 Introduction

In the past decades, significant progress has been made in computational modeling of damage and fracture processes in quasi-brittle materials such as concrete and masonry. Most of the available models are continuum models which require very fine finite element meshes in the vicinity of a crack or localization zone. Discrete models are consistent with the physical observation of a discrete crack as a displacement jump across a discontinuity surface. The extended finite element approach belongs to this class of models (see, for example, [2,4,10,17]). In this formulation, cracks are not restricted to the finite element boundaries; instead, they can freely run through the finite element mesh. As a result, coarser meshes can be used, rendering these models suitable for larger scale computations. However, an embedded discontinuity in a coarse mesh cannot accurately represent the energy consumed by micro-crack branching prior to the formation of the macro-crack. A better characterization of the whole failure process can be achieved by combining continuous and discontinuous theories into a global macroscopic framework.
This idea has been successfully pursued by many authors (see, for example, [8,12,14,16]), nevertheless some issues remain. It is for example not clear when a discrete

crack should be introduced. Some authors introduce a traction-free discontinuity at the final stages of failure. In this case the continuum model governs the softening behavior (see, for example, [16]). Other authors make use of the cohesive zone assumption (see [1,6]). Here a traction-separation model governs the non-linear behavior in the fracture process zone and the continuum can remain elastic at all times (see, for example, [17]). Both approaches have in common that a single moment exists at which the continuum model is replaced by a discrete model. The distinct feature of the model proposed in the present paper is that this transition takes place gradually. A damage-type cohesive law allows using the constitutive model for the continuum in the undamaged material bonds at the process zone, whereas the damaged part of the crack is traction-free. As damage grows, material bonds are broken and a macro-crack is formed. This conceptually different cohesive zone model is formulated irrespective of the underlying model for the undamaged material. The gradual transition ensures that the stress at a point varies in a continuous manner during the entire solution trajectory. This concept is known as 'time continuity', and was introduced by Papoulia et al. [13] as a prerequisite for robustness of a continuous-discontinuous framework.

The paper starts by introducing the discrete constitutive equations (Section 3.1) and the continuum material model (Section 3.2). The implementation in a strong discontinuity framework is discussed in section 4. In section 5 several aspects of the model are highlighted by means of numerical examples.

3 Constitutive equations

3.1 Discrete constitutive model

3.1.1 Damage-based discrete constitutive equation

Consider an infinitesimal part of a plane dA with unit normal $\mathbf{n}$ in a structure or structural component (Figure 1a). The tractions $\mathbf{t}$ acting on this plane are obtained as

$$\mathbf{t} = \boldsymbol{\sigma}\mathbf{n} \tag{1}$$

where $\boldsymbol{\sigma}$ is the second order continuum stress tensor. Tensile tractions have a positive sign. Suppose that micro-cracks and -voids start to grow on this infinitesimal plane (Figure 1b). In that case, we can quantify the ratio between the damaged area and the total area with a scalar damage variable ω, ranging from zero to one. Zero damage corresponds to the undamaged bulk material, whereas ω equals one upon complete separation along the crack plane. The bulk material will, in general, include pores, deficiencies and irregularities. All these 'imperfections' are randomly distributed in the material. As a result, they are not considered as 'damage' but rather as a characteristic of the continuum.

Tractions can only be transferred in the material through the undamaged material bonds. We assumed that the micro-voids and -cracks influence the stress field in the surrounding continuum material only locally. If the micro-voids and -cracks grow and coalesce into macro-cracks, the surrounding material will relax and all stresses will vanish. Hence, it is reasonable to assume that the effective tractions in the material bonds $\mathbf{t}^{eff}$, acting on the undamaged part of the infinitesimal area dA, equal the homogenized stresses in the

surrounding continuum, projected on the plane and acting on the same area (Figure 1c), or

$$\boldsymbol{\sigma}\mathbf{n}\,dA = \mathbf{t}^{eff}\left(1-\omega\right)dA \;\text{ for }\; 0 \le \omega \le 1 \tag{2}$$

Before any damage occurs, the effective tractions equal the continuum stresses (Eq. 2 with $\omega = 0$). As damage grows, the active area decreases and higher effective tractions are needed to maintain equilibrium with the continuum stresses. The redistribution of the tractions causes additional deformations in the undamaged material bonds. Therefore, the effective traction can be additively decomposed into two terms, namely, (i) the initial traction prior to damage growth and (ii) the traction related to the damage-induced elongation of the material bond:

$$\mathbf{t}^{eff} = \boldsymbol{\sigma}\mathbf{n} + \gamma^{-1}\mathbf{Q}\llbracket\tilde{\mathbf{u}}\rrbracket \tag{3}$$

where $\mathbf{Q} = \mathbf{nDn}$ is the acoustic tensor, with $\mathbf{D}$ a 4th order constitutive tensor describing the constitutive behavior of the bulk material, $\llbracket\tilde{\mathbf{u}}\rrbracket$ is a displacement jump corresponding to the elongation of the material bond, γ is one unit length and follows from dimensional analysis. The acoustic tensor represents the projection of the bulk behavior onto the discontinuity plane. If the discontinuity plane corresponds to a material interface, we can either use the acoustic tensor of the bond material (i.e. the glue) or - in absence of a bonding material - the acoustic tensor of the coupled system:

$$\mathbf{Q} = 2\left(\mathbf{Q}_1^{-1} + \mathbf{Q}_2^{-1}\right)^{-1} \tag{4}$$

where $\mathbf{Q}_1$ and $\mathbf{Q}_2$ represent the acoustic tensors of both materials. The latter choice implies a perfect bond between both. In case of two equal materials $\mathbf{Q} = \mathbf{Q}_1 = \mathbf{Q}_2$.

Combining equations (1-3) finally yields the constitutive equation for the cohesive zone:

$$\mathbf{t} = \left(1-\omega\right)\left[\boldsymbol{\sigma}\mathbf{n} + \gamma^{-1}\mathbf{Q}\llbracket\tilde{\mathbf{u}}\rrbracket\right] \tag{5}$$

Equation (5) represents the gradual degradation from a continuum to a discrete state. Figure 2 illustrates this equation in a graphical way for a one dimensional case with a specific choice of the model parameters. Upon initiation of the crack, the crack width and the damage variable equal zero and equation (1) is recovered: the material behaves as if no discontinuity were present. As damage grows, the relative contribution of the discrete component of the total traction gains importance over the continuum component (Figure 2b, dashed line). At rupture, the damage variable becomes one and the traction forces become zero. This corresponds to a traction-free discontinuity.

If the loading were reversed before rupture occurred, the damage would cease to grow, but equation (5) can still be used without modification to obtain the total traction vector. As the stress decreases, both crack width and total traction will decrease, and finally become zero.

3.1.2 Damage evolution

The proposed discrete constitutive equation needs to be supplemented with a proper damage criterion and a suitable damage evolution law.

Criteria for damage growth are either stress-based or strain-based. In a discrete setting, the corresponding criteria are traction-based or displacement jump-based. Considering that (i) the discrete law (Eq. 5) depends on the equilibrium between the effective tractions in the undamaged material bonds and the homogenized stresses in the surrounding

continuum matrix, and that (ii) the corresponding strain field is unbounded if localization occurs in a band of zero width, it is clear that a traction-based damage criterion is preferred in this formulation. In this study, a rankine-type damage criterion is adopted:

$$f\left(\mathbf{t}^{eff},\omega\right)=t^{eff,eq}-\kappa\leq 0 \tag{6}$$

in which $t^{eff,eq}\left(\mathbf{t}^{eff}\right)$ is an equivalent traction, expressed as a function of the effective tractions, and $\kappa(\omega)$ is the residual strength of the damaged material. For mode I dominated failure, the following expression for the equivalent traction is found suitable:

$$t^{eff,eq}=\mathbf{t}^{eff}\cdot\mathbf{n} \tag{7}$$

A simple, yet flexible, expression for κ is given by

$$\kappa(\omega)=f_t^0+\left(f_t^1-f_t^0\right)\omega^n \tag{8}$$

with $f_t^0>0$ the tensile strength of the virgin bulk material, $f_t^1\geq 0$ the residual tensile strength of the damaged bulk material, and $n\geq 0$ a hardening/softening exponent.

The damage evolution law is defined by the Kuhn-Tucker conditions:

$$\dot{\omega}\geq 0,\ f\leq 0,\ \dot{\omega}f=0 \tag{9}$$

supplemented with the consistency condition:

$$\dot{\omega}\dot{f}=0 \tag{10}$$

The damage evolution law is not explicitly given in terms of e.g. the equivalent traction. The updated values of the damage and the corresponding traction vector and crack width are obtained via return mapping, similar to plasticity. This algorithm will be discussed in more detail in section 4.7.

3.1.3 Determination of the mode I fracture energy

The fracture energy is defined as:

$$G_f=\int_0^{+\infty}\mathbf{t}\cdot d[\![\tilde{\mathbf{u}}]\!] \tag{11}$$

Upon crack propagation, the traction can be expressed as:

$$\mathbf{t}=(1-\omega)\mathbf{t}^{eff}=(1-\omega)\kappa\frac{\mathbf{m}}{\mathbf{m}\cdot\mathbf{n}} \tag{12}$$

where $\mathbf{m}$ is a unit vector pointing in the direction of the displacement jump. The form of equation (12) is closely related to the expression for the equivalent effective traction (Eq. 7) and accordingly does not hold for pure mode II loading ($\mathbf{m}\cdot\mathbf{n}=0$).

The displacement jump can be expressed as:

$$[\![\tilde{\mathbf{u}}]\!]=\omega\kappa\gamma\mathbf{Q}^{-1}\frac{\mathbf{m}}{\mathbf{m}\cdot\mathbf{n}} \tag{13}$$

Equation (13) is derived from (5), after eliminating $\boldsymbol{\sigma}\mathbf{n}$ by means of (1) and $\mathbf{t}$ by means of (12). Substituting equations (12) and (13) in (11) and taking into account that for pure mode I loading $\mathbf{m}=\mathbf{n}$, we obtain the mode I fracture energy G_f^I:

$$\begin{aligned}G_f^I&=\int_0^1(1-\omega)\kappa\mathbf{n}\cdot\left(\omega\frac{\partial\kappa}{\partial\omega}+\kappa\right)\gamma\mathbf{Q}^{-1}\mathbf{n}\,d\omega\\&=\left(\mathbf{n}\cdot\mathbf{Q}^{-1}\mathbf{n}\right)\gamma\int_0^1(1-\omega)\left(\omega\frac{\partial\kappa}{\partial\omega}+\kappa\right)\kappa\,d\omega\end{aligned} \tag{14}$$

If κ is defined according to equation (8) the expression becomes:

$$G_f^I = \left(\mathbf{n}\cdot\mathbf{Q}^{-1}\mathbf{n}\right)\gamma\frac{\left(2n^2\left(f_t^0\right)^2+2nf_t^0f_t^1+\left(n+1\right)\left(f_t^1\right)^2\right)}{2\left(n+1\right)\left(2n+1\right)} \tag{15}$$

In the special case that $f_t^1 = f_t^0 = f_t$, this expression reduces to $G_f^I = \left(\mathbf{n}\cdot\mathbf{Q}^{-1}\mathbf{n}\right)\gamma\frac{1}{2}f_t^2 = \frac{1}{2}\left(\left\|\tilde{\mathbf{u}}_{\max}\right\|\cdot\mathbf{n}\right)f_t$, which corresponds to the classical case of linear softening in e.g. interface elements. $\left\|\tilde{\mathbf{u}}_{\max}\right\|$ is obtained from equation (13) with $\omega = 1$. Note that no softening parameter (n) is required in case $f_t^1 = f_t^0 = f_t$.

3.1.4 *Crack initiation and propagation*

Finally, we need to define when a discontinuity should initiate or propagate. We have already shown that upon crack initiation, the discrete constitutive equation (Eq. 5) reduces to traction equilibrium on the potential crack plane (Eq. 1). In the same line of reasoning, the discrete damage criterion (Eq. 6) corresponds to the following initiation criterion:

$$f = \sigma_i - \kappa^0 \le 0 \tag{16}$$

with σ_i the i$^{\text{th}}$ principal stress and $\kappa^0 = \kappa\left(\omega = 0\right)$. If equation (16) is violated at a material point, a new crack segment is introduced with the normal pointing in the (critical) principal stress direction.

It is recommended to determine the direction of the discontinuity based on the non-local stress tensor $\bar{\boldsymbol{\sigma}}$, calculated as a weighted average of stresses using a Gaussian weighting function w (see [7]):

$$\bar{\boldsymbol{\sigma}} = \frac{\int_\Omega w\boldsymbol{\sigma}d\Omega}{\int_\Omega w d\Omega} \text{ with } w = \frac{1}{\left(2\pi\right)^{3/2}l^3}\exp\left(-\frac{r^2}{2l^2}\right) \tag{17}$$

where r is the distance to the crack tip and l the influence length, taken approximately equal to three times the element size (see [17]).

3.2 Continuum constitutive model

The framework has been formulated irrespective of the constitutive model used for the continuum. To avoid confusion between softening behavior caused by either the continuum or the discrete constitutive model, we use a linear elastic bulk model according to:

$$\boldsymbol{\sigma} = \mathbf{D}\boldsymbol{\varepsilon} \tag{18}$$

with $\mathbf{D} = \lambda\mathbf{1}\otimes\mathbf{1} + 2\mu\mathbf{I}$ the elasticity tensor, $\mathbf{1}$ and $\mathbf{I}$ the second and fourth order unit tensors, and λ and μ the lamé constants. $\boldsymbol{\varepsilon}$ is the second order strain tensor. The softening response is thus due to the discrete constitutive model.

4 Implementation in a strong discontinuity framework

4.1 Kinematics

Figure 3a illustrates a body Ω crossed by a displacement discontinuity Γ_d. Using the PU-concept (see [5]), the total displacement field is given by:

$$\mathbf{u} = \hat{\mathbf{u}} + H_{\Gamma_d}\tilde{\mathbf{u}} \tag{19}$$

where $\hat{\mathbf{u}}$ and $\tilde{\mathbf{u}}$ are smooth, continuous functions on Ω and H_{Γ_d} is the Heaviside step function corresponding to and centered at the discontinuity Γ_d (Figure 3b). The Heaviside function is equal to one for all points $x \in \Omega^+$ and zero for all other points $x \in \Omega^-$.

The total strain field $\boldsymbol{\varepsilon}^{tot}$ (Figure 3c) can be found by taking the symmetric gradient of the displacement field:

$$\boldsymbol{\varepsilon}^{tot} = \nabla^s \mathbf{u} = \nabla^s \hat{\mathbf{u}} + H_{\Gamma_d}\nabla^s \tilde{\mathbf{u}} + \delta_{\Gamma_d}\left(\tilde{\mathbf{u}} \otimes \mathbf{n}\right)^s \tag{20}$$

where $\mathbf{n}$ is the normal to the discontinuity and δ_{Γ_d} is the Dirac delta distribution, centered at the discontinuity. The Dirac delta distribution is the derivative of the Heaviside step function and is nonzero only for the points on the discontinuity.

4.2 Strong form

The equilibrium equation in absence of body forces reads:

$$\nabla \cdot \boldsymbol{\sigma} = 0 \text{ in } \Omega \tag{21}$$

The natural boundary conditions are given by:

$$\boldsymbol{\sigma}\bar{\mathbf{n}} = \bar{\mathbf{t}} \text{ on } \Gamma_t \tag{22a}$$

$$\boldsymbol{\sigma}\mathbf{n} = -\mathbf{t}_d^+ \text{ on } \Gamma_d^+ \tag{22b}$$

$$\boldsymbol{\sigma}\mathbf{n} = \mathbf{t}_d^- \text{ on } \Gamma_d^- \tag{22c}$$

where $\boldsymbol{\sigma}$ is the second order stress tensor, $\bar{\mathbf{n}}$ is the outward normal to the body, $\mathbf{n}$ is the outward normal to Ω^- on Γ_d^-. The minus sign indicates that the direction of the tractions $\mathbf{t}_d^+$ is opposite to the direction of $\mathbf{n}$. Tensile tractions are taken positive.

The essential boundary conditions are:

$$\mathbf{u} = \bar{\mathbf{u}} \text{ on } \Gamma_u \tag{23}$$

4.3 Weak form

Weak equilibrium statement is written as:

$$\int_\Omega \mathbf{w} \cdot \left(\nabla \cdot \boldsymbol{\sigma}\right) d\Omega = 0 \tag{24}$$

Which must hold for all admissible variations of displacement $\mathbf{w}$. Following a Galerkin approach (i.e. taking the space of admissible variations the same as the actual displacements) leads, after standard manipulations, to the following set of variational statements:

$$\int_\Omega \nabla^s \hat{\mathbf{w}} : \boldsymbol{\sigma} d\Omega = \int_{\Gamma_d^-} \hat{\mathbf{w}} \cdot \mathbf{t}_d^- d\Gamma + \int_{\Gamma_d^+} \hat{\mathbf{w}} \cdot \mathbf{t}_d^+ d\Gamma + \int_{\Gamma_t} \hat{\mathbf{w}} \cdot \bar{\mathbf{t}} d\Gamma \tag{25a}$$

$$\int_\Omega H_{\Gamma_d} \nabla^s \tilde{\mathbf{w}} : \boldsymbol{\sigma} d\Omega = \int_{\Gamma_d^-} H_{\Gamma_d}^- \tilde{\mathbf{w}} \cdot \mathbf{t}_d^- d\Gamma + \int_{\Gamma_d^+} H_{\Gamma_d}^+ \tilde{\mathbf{w}} \cdot \mathbf{t}_d^+ d\Gamma + \int_{\Gamma_t} H_{\Gamma_d} \tilde{\mathbf{w}} \cdot \bar{\mathbf{t}} d\Gamma \quad (25b)$$

4.4 Discretized form

Nodes whose support is crossed by a discontinuity are assigned a regular and an enhanced set of degrees of freedom, denoted with $\mathbf{a}$ and $\mathbf{b}$, respectively. The discretized format of equation (19) then reads:

$$\mathbf{u} = \mathbf{N}\mathbf{a} + H_{\Gamma_d} \mathbf{N}\mathbf{b} \quad (26)$$

Where $\mathbf{N}$ is the array containing the finite element shape functions. The strain field can be discretized in a similar fashion using the interpolation matrix $\mathbf{B}$. For elements with only regular degrees of freedom $\mathbf{a}$, the problem fields are discretized in the standard way.

The discretized format of the weak governing equations reads:

$$\int_\Omega \mathbf{B}^T \boldsymbol{\sigma} d\Omega = \int_{\Gamma_t} \mathbf{N}^T \bar{\mathbf{t}} d\Gamma \quad (27a)$$

$$\int_\Omega H_{\Gamma_d} \mathbf{B}^T \boldsymbol{\sigma} d\Omega = \int_{\Gamma_d^+} H_{\Gamma_d}^+ \mathbf{N}^T \mathbf{t}_d^+ d\Gamma + \int_{\Gamma_t} H_{\Gamma_d} \mathbf{N}^T \bar{\mathbf{t}} d\Gamma \quad (27b)$$

where we used the relations $\mathbf{t}_d^+ = -\mathbf{t}_d^-$ and $H_{\Gamma_d}^- = 0$.

4.5 Discretization of the constitutive relations

The stress in the bulk material (see Eq. 18) is expressed in terms of the nodal displacements as:

$$\boldsymbol{\sigma} = \mathbf{D}\boldsymbol{\varepsilon} = \mathbf{D}\left(\mathbf{B}\mathbf{a} + H_{\Gamma_d} \mathbf{B}\mathbf{b}\right) \quad (28)$$

If the shape functions were able to exactly represent the displacement field, the true stress tensor could be computed by means of equation (28). In practice, the interpolation functions are a limited subset of the entire solution space, and equation (28) provides only an approximate value for the local stress tensor at a point. However, the proposed discrete model, as described in Section 3.1, relies on the knowledge of the true local stress tensor to ensure a gradual transition from a continuum to a discrete state. Simply inserting the discretized expressions for displacement and stress in equation (5) could lead to inaccurate results, especially in the study of dynamic problems or in case a non-linear constitutive model for the bulk material is used. By casting the discrete traction law in a different format prior to discretization, the successful use of the method is no longer restricted to linear elastic, quasi-static simulations.

We first make a distinction between two types of transitions: namely (i) the transition to strong discontinuity kinematics (i.e. the insertion of a discontinuity in the displacement field) and (ii) the transition from a continuous to a discontinuous state as described by the cohesive model. The former corresponds to the moment at which the propagation criterium (Eq. 16) at a point is violated and a strong discontinuity is inserted with zero damage ($\omega = 0$); the latter relates to the process of damage evolution ($0 < \omega \leq 1$).

4.5.1 Transition to strong discontinuity kinematics

From equation (13) it is clear that a jump in the displacement field cannot exist in absence of damage ($\omega = 0$). The use of strong discontinuity kinematics (with a Heaviside enrichment) is therefore not required. However, the displacement field does not need to

be smooth, hence the strain field can exhibit a jump across the discontinuity, as long as equilibrium is satisfied:

$$\llbracket\boldsymbol{\sigma}\rrbracket\mathbf{n} = \mathbf{0} \tag{29}$$

A discontinuity in the strain field is termed a weak discontinuity. In the corresponding description of the displacement field, the distance function is usually used as enrichment function. In contrast with strong discontinuity kinematics, weak discontinuity kinematics does not give rise to integrals over the discontinuity in the weak form. Hence it is not needed to provide an explicit expression for the cohesive traction if $\omega = 0$.

4.5.2 *Transition from a continuous to a discontinuous state*

Since the damage variable is nonzero during the transition, we can eliminate the continuum stress from equation (5) by means of equation (1):

$$\mathbf{t} = \left(\frac{1-\omega}{\gamma\omega}\right)\mathbf{Q}\llbracket\tilde{\mathbf{u}}\rrbracket \text{ with } 0 < \omega \leq 1 \tag{30}$$

This expression allows computing the traction vector solely based on the displacement jump. The dependency on the continuum stress tensor is implicitly present.

At this point, it is worthwhile to make a comparison with another cohesive law used in a strong discontinuity context. Therefore, we substitute the damage variable by $\omega = \left(1+\gamma\left(1-\varpi\right)\right)^{-1}$:

$$\mathbf{t} = \left(1-\varpi\right)\mathbf{Q}\llbracket\tilde{\mathbf{u}}\rrbracket \text{ with } -\infty < \varpi \leq 1 \text{ m}^{-1} \tag{31}$$

Equation (31) has been obtained by Oliver [11], by performing a strong discontinuity analysis of the isotropic damage model of Simo [15]. As compared to our formulation, two important differences have to be noted: (i) the dimensional damage variable ϖ ranging from $-\infty$ m^{-1} to one m^{-1} is physically less relevant than the dimensionless variable ω ranging from zero to one, and (ii) the singularity at $\omega = 0$ (in Eq. 30) arises from an attempt to avoid errors introduced by the discretization, whereas the singularity at $\varpi = -\infty$ m^{-1} (in [11]) results from the presence of a Dirac delta distribution in the strain field for strong discontinuity kinematics.

4.6 Linearized and discretized form

After linearization, the system of equations becomes:

$$\begin{bmatrix} \mathbf{K}^i_{aa} & \mathbf{K}^i_{ab} \\ \mathbf{K}^i_{ba} & \mathbf{K}^i_{bb} \end{bmatrix} \begin{bmatrix} \delta\mathbf{a}^{i+1} \\ \delta\mathbf{b}^{i+1} \end{bmatrix} = \begin{bmatrix} \mathbf{f}^i_{ext,a} \\ \mathbf{f}^i_{ext,b} \end{bmatrix} - \begin{bmatrix} \mathbf{f}^i_{int,a} \\ \mathbf{f}^i_{int,b} \end{bmatrix} \tag{32}$$

With

$$\mathbf{K}_{aa} = \int_\Omega \mathbf{B}^T\mathbf{D}\mathbf{B}d\Omega \tag{33a}$$

$$\mathbf{K}_{ba} = \mathbf{K}^T_{ab} = \int_\Omega H_{\Gamma_d}\mathbf{B}^T\mathbf{D}\mathbf{B}d\Omega \tag{33b}$$

$$\mathbf{K}_{bb} = \int_\Omega H_{\Gamma_d}\mathbf{B}^T\mathbf{D}\mathbf{B}d\Omega + \int_{\Gamma_d^+} H_{\Gamma_d}\mathbf{N}^T\mathbf{T}^+\mathbf{N}d\Gamma \tag{33c}$$

$$\mathbf{f}_{ext,a} = \int_{\Gamma_t} \mathbf{N}^T\bar{\mathbf{t}}d\Gamma \tag{33d}$$

$$\mathbf{f}_{ext,b} = \int_{\Gamma_t} H_{\Gamma_d}\mathbf{N}^T\bar{\mathbf{t}}d\Gamma \tag{33e}$$

$$\mathbf{f}_{int,a} = \int_{\Omega} \mathbf{B}^T \boldsymbol{\sigma} d\Omega \tag{33f}$$

$$\mathbf{f}_{int,b} = \int_{\Omega} H_{\Gamma_d} \mathbf{B}^T \boldsymbol{\sigma} d\Omega + \int_{\Gamma_d^+} H_{\Gamma_d} \mathbf{N}^T \mathbf{t}^+ d\Gamma \tag{33g}$$

The superscript i indicates the iteration counter in the global iterative procedure. The matrix $\mathbf{T}$ follows from the linearization of the discrete model and is given by:

$$\mathbf{T} = \left(\frac{1-\omega}{\gamma\omega} \right) \mathbf{Q} - \frac{1}{\gamma\omega} \frac{\mathbf{t}^{eff} \otimes \mathbf{n}\mathbf{Q}}{\kappa + \omega \dfrac{\partial \kappa}{\partial \omega}} \quad \text{where } 0 < \omega \leq 1 \tag{34}$$

in the case of loading. For unloading and reloading, the discrete tangent becomes

$$\mathbf{T} = \left(\frac{1-\omega}{\gamma\omega} \right) \mathbf{Q} \quad \text{where } 0 < \omega \leq 1 \tag{35}$$

Although the above derivation is theoretically sound, the use of equations (34) or (35) will have a negative impact on the condition number of the stiffness matrix for very small values of the damage variable. A pragmatic approach is followed. Equations (34) and (35) are used if the damage variable exceeds a predefined threshold ω_{crit}, where ω_{crit} is a real positive number close to zero. Below ω_{crit}, it is more accurate to use the original expression for the discrete law (Eq. 5) where the local stress tensor is approximated as:

$$\boldsymbol{\sigma}^{approx.} = \tfrac{1}{2} \left(\boldsymbol{\sigma}^- + \boldsymbol{\sigma}^+ \right) \tag{36}$$

In equation (36) $\boldsymbol{\sigma}^-$ and $\boldsymbol{\sigma}^+$ are the stress tensors, evaluated at the negative and positive side of the discontinuity. The tangent for $0 \leq \omega < \omega_{crit}$ follows directly from the linearisation of equation (5), and contains contributions to $\mathbf{K}_{ba}$ and $\mathbf{K}_{bb}$. Since the approximated expressions can be used for $\omega = 0$, there is no need to employ weak discontinuity kinematics. The validity of this approximation is verified in Section 5.3.

4.7 Return mapping

First, the system of equations (Eq. 32) is solved using the previous converged value of the damage variable (trial state). Next, the effective traction is computed for each point on the discontinuity and the admissibility of the stress state is verified. If the damage criterion is satisfied, i.e. $f \leq 0$, the stress state is admissible and the trial state is the real state. However, if the damage criterion is violated ($f > 0$), the damage variable needs to be updated.

The new damage variable can be found as the root of the damage criterion (Eq. 6). Generally, κ can be a non-linear function of ω, and an explicitly solving for ω is not possible. Therefore a local iterative scheme should be applied (e.g. Newton-Raphson scheme):

$$f^{j+1} = f^j + \left. \frac{\delta f}{\delta \omega} \right|_{\omega^j} \left(\omega^{j+1} - \omega^j \right) + R^2 \tag{37}$$

Where the superscript j denotes the counter in the local iterative procedure. Omitting the terms of second order and higher and elaborating the derivative yields:

$$f^{j+1} = f^j + \left(\left. \frac{\delta t^{eff,eq}}{\delta \omega} \right|_{\omega^j} - \left. \frac{\delta \kappa}{\delta \omega} \right|_{\omega^j} \right) \left(\omega^{j+1} - \omega^j \right) \tag{38}$$

The term $\frac{\delta\kappa}{\delta\omega}$ represents the change in residual strength of the material bonds during damage evolution, and can be obtained by derivation of equation (8). The term $\frac{\delta t^{eff,eq}}{\delta\omega}$ describes the variation of the effective stresses upon increasing damage. In the proposed discrete model, the evolution of damage is not explicitly given in terms of the equivalent traction. An expression for $\delta t^{eff,eq}$ can be obtained under the assumption that the total strain $\boldsymbol{\varepsilon}_{\Gamma_d}^{tot}$ at the discontinuity remains constant during a global iteration.

In analogy with the additive decomposition of the effective traction vector (see Eq. 3), the strain field at the discontinuity $\boldsymbol{\varepsilon}_{\Gamma_d}^{tot}$ is assumed to consist of two terms, namely, (i) an initial strain prior to the development of a strong discontinuity (i.e. with $[\![\tilde{\mathbf{u}}]\!]=0$) and (ii) a strain-like term related to the displacement jump at the discontinuity:

$$\boldsymbol{\varepsilon}_{\Gamma_d}^{tot} = \boldsymbol{\varepsilon} + \zeta\left([\![\tilde{\mathbf{u}}]\!]\otimes\mathbf{n}\right)^s \tag{39}$$

Comparison with equation (20) points out that $\boldsymbol{\varepsilon}=\nabla^s\hat{\mathbf{u}}+H_{\Gamma_d}\nabla^s\tilde{\mathbf{u}}$ is the 'continuum' strain field and $\zeta\left([\![\tilde{\mathbf{u}}]\!]\otimes\mathbf{n}\right)^s$ with $\zeta=\delta_{\Gamma_d}$ is the 'discrete' contribution. The latter is theoretically unbound due to the presence of the Dirac delta function. In the spirit of strong discontinuity analysis, we consider a discontinuity band of bandwidth h, instead of a discontinuity plane with zero thickness. ζ can than be defined as:

$$\zeta=\begin{cases}0 & \Leftrightarrow x\notin\left[-\frac{1}{2}h,\frac{1}{2}h\right]\\ h^{-1} & \Leftrightarrow x\in\left[-\frac{1}{2}h,\frac{1}{2}h\right]\end{cases} \tag{40}$$

In the limit of $h\to 0$ we have $\zeta=\delta_{\Gamma_d}$. Pre- and post-multiplying equation (39) with the stiffness $\mathbf{D}$ and the normal to the discontinuity $\mathbf{n}$, respectively, leads to:

$$\mathbf{D}\boldsymbol{\varepsilon}_{\Gamma_d}^{tot}\mathbf{n} = \boldsymbol{\sigma}\mathbf{n} + \zeta\mathbf{Q}[\![\tilde{\mathbf{u}}]\!] \tag{41}$$

where we made use of the constitutive equation (Eq. 18) and the definition of the acoustic tensor. Rearranging yields:

$$\mathbf{D}\boldsymbol{\varepsilon}_{\Gamma_d}^{tot}\mathbf{n} = \left(1-\zeta\gamma\right)\boldsymbol{\sigma}\mathbf{n} + \zeta\gamma\left(\boldsymbol{\sigma}\mathbf{n}+\gamma^{-1}\mathbf{Q}[\![\tilde{\mathbf{u}}]\!]\right) \tag{42}$$

Note that the product $\zeta\gamma$ is dimensionless. Making use of equations (1), (3) and (5) we obtain:

$$\mathbf{D}\boldsymbol{\varepsilon}_{\Gamma_d}^{tot}\mathbf{n} = \left(1-\omega+\zeta\gamma\omega\right)\mathbf{t}^{eff} \tag{43}$$

Under the assumption that $\boldsymbol{\varepsilon}_{\Gamma_d}^{tot}$ is kept constant during return mapping, the partial derivative of the effective traction vector with respect to damage can thus be expressed as:

$$\frac{\partial\mathbf{t}^{eff}}{\partial\omega} = \left(\frac{1-\zeta\gamma}{1-\omega+\zeta\gamma\omega}\right)\mathbf{t}^{eff} \tag{44}$$

Inserting equations (8) and (44) in (38) yields:

$$f^{j+1} = f^{j} - \left(\left(\frac{1-\zeta\gamma}{1-\omega+\zeta\gamma\omega}\right)t^{eff,eq,j} + n\left(f_t^1-f_t^0\right)\left(\omega^j\right)^{n-1}\right)\left(\omega^{j+1}-\omega^j\right) \tag{45}$$

In the limit of $h \to 0$ we have $\zeta = \delta_{\Gamma_d}$ and (45) becomes

$$f^{j+1} = f^j - \left(\frac{1}{\omega^j} t^{eff,eq,j} + n\left(f_t^1 - f_t^0 \right) \left(\omega^j \right)^{n-1} \right) \left(\omega^{j+1} - \omega^j \right) \tag{46}$$

We find the updated damage variable as the root of equation (46), after setting $f^{j+1} = 0$. However, since this expression is singular for $\omega = 0$, we prefer using equation (45) with a value of $\zeta \gg 1$. This choice influences the rate of convergence of the local iterative procedure, not the global equilibrium state. ζ only appears in the return mapping scheme, not in the tangent. Therefore, selecting a high value for ζ does not render the system ill-conditioned. The updated damage variable obeys the Kuhn-Tucker conditions since $f^{j+1} = 0$ and $\Delta\omega > 0$ if $\zeta > 1$.

5 Numerical examples

In this section three different numerical examples are presented. First, a uniaxial tension test on a 3 by 3 element mesh is studied. A full parametric study of the model is performed and the simplicity of the example allows observing the influence of the individual parameters. Next, aspects of mesh objectivity are analyzed by means of a four point bending test. Finally, the applicability of the model in a multi-material setting is illustrated by means of a mode I double cantilever beam test.

5.1 Uniaxial tension

A 2D uniaxial tensile test is performed on a square sample with an edge length of 0.03 m (Figure 4). The sample is discretized with 9 square bilinear elements. Nodes on the left boundary are clamped in x-direction. Nodes at the right boundary are forced to move in x-direction at a fixed rate. Two additional constraints in y-direction prevent rigid body motions. A strong discontinuity with normal pointing in the positive x-direction is inserted in the 3 middle elements. The discontinuity is damage-free at the beginning of the computations. Plane stress conditions are assumed. The Poisson ratio is taken equal to zero to simplify interpretation of the results. The influence of changing the Young's modulus, tensile strength, residual tensile strength and hardening exponent are studied. Table 1 gives an overview of the investigated parameters. Please note that G_f^I is not an explicit model parameter, but is being calculated from equation (15).

Figure 5a shows the influence of variations in stiffness. It is observed that the stiffer the material is, the more brittle it behaves. A higher tensile strength influences the peak load, but does not affect the slope of the loading and softening branch (Figure 5b). If tensile strength and residual tensile strength are given distinct values, both slope and shape of the softening branch are altered (Figure 5c). Choosing $f_t^1 > f_t^0$ leads to a more ductile response, whereas the opposite choice, $f_t^1 < f_t^0$, results in more brittle failure or even snap-back if $f_t^1 < \left(n/(n+1) \right) f_t^0$. Snap-back could not be illustrated in Figure 5c since the test is performed under displacement control. Figure 5d illustrates the effect of the softening parameter. If $n > 1$, the slope of the softening branch becomes more convex. A more concave shape is found for $0 < n < 1$. Essential parameters E and f_t^0 can be

identified experimentally from a uni-axial tensile test. Secondary parameters f_t^1 and n require inverse analysis. Adopting different expressions for κ (instead of Eq. 8) and $\boldsymbol{\sigma}$ (instead of Eq. 18) allows describing the behavior of a wide range of materials.

5.2 Four-point bending

A four-point bending test on a notched beam is used to prove mesh objectivity of the response. The beam has a length of 0.24 m and cross-sectional dimensions 0.048 m x 0.024 m (height x depth). The notch has a width of 0.004 m, a depth of 0.008 m and a circular tip. The distance between the two supports is 0.2 m and between the loading points 0.1 m. A Young's modulus of 10 GPa, a Poisson's ratio of 0.2, a tensile strength of 3 MPa, a residual tensile strength of 2 MPa and a softening exponent of 0.6 were selected. These values are representative for meule sandstone. The simulations were performed in 2D under plane stress assumptions. Meshes were constructed for two element types (bilinear quadrilateral and linear triangle) and for three levels of mesh refinement (572, 1596 and 5604 dofs, respectively). The six meshes are depicted in Figure 6. A new crack segment is introduced at the end of a load step, if the failure criterium is violated at the crack tip. In this way, crack path continuity is easily enforced. Afterwards global equilibrium is reevaluated. The procedure is repeated until the initiation criterion is no longer met. New crack segments cross the entire element at once. Displacement control was applied.

The results of the mesh sensitivity analysis are presented in Figure 7 as 'force' versus 'opening at the notch' diagrams. Comparing the three structured meshes based on quadrilateral elements (Figure 7a) it is seen that the meshes with 1596 and 5604 dofs yield almost the same response. The mesh with 572 dofs is too coarse to capture the actual behavior.

For the meshes based on triangular elements, load drops are observed in the softening branch each time a new crack segment is introduced (Figure 7b). The presence of load drops is related to the constant strain property of the T3-element. Since we use a linear elastic constitutive relation, the stress field is constant over the element as well. Therefore, the stress field in the cohesive zone is not decaying gradually, but in a stepwise manner. Upon propagation, the stress field undergoes a stepwise change as well, and a load drop is observed. Upon mesh refinement, the number of elements over the cohesive zone increases, allowing a more accurate representation of the stress field in the cohesive zone. As a result, the number of load drops increases, but their magnitude decreases. The mesh with 5604 dofs yields the same response as the two finest meshes with quadrilateral elements.

The computations were repeated with smaller load steps. At coinciding loading points an identical response was obtained. For this example the size of the load step did not influence the robustness of the algorithm. If a nonlinear model is chosen to represent the bulk behaviour, it can be expected that there exists an upper bound to the load step.

5.3 Double cantilever beam

As a final example, a comparison between the proposed cohesive zone model and classical interface elements is presented by means of a mode I double cantilever beam test (DCB). A composite beam of 0.0025 m length and 0.0005 m height is subjected to a splitting loading (See Figure 8). The beam consists of two layers with equal height: a

softer upper layer on a stiffer base layer. Both layers have a Poisson's ratio of 0.3 and a tensile strength of 1 MPa. The stiffness of the base layer is 10 GPa. The stiffness of the upper layer is taken 5, 10, 20 and 50 times lower. The material interface is modeled in two different ways. First using the proposed cohesive zone model ($E = 10\,\text{GPa};\ \nu = 0;$ $f_t^0 = 1\,\text{MPa};\ \ f_t^1 = 1\,\text{MPa};\ \ n = 1$). This choice of parameters yields a linear softening behavior with a fracture energy of 50 N/m. Alternatively, interface elements employing a linear softening law are used. Although the use of a dummy stiffness can be avoided by e.g. initially constraining the interfaces (see [3]), we make use of classical interface elements with a dummy stiffness of 1.0E6 GPa. The tensile strength and fracture energy are taken 1 MPa and 50 N/m, respectively. The beam consists of 125 bilinear elements for the X-FEM simulation and 150 bilinear elements for the simulation with interface elements. Both meshes have 300 dofs. Plane stress conditions are assumed.

In Figure 9, the applied load F is plotted against the vertical displacement of the loading point. Dashed lines represent the solution with interface elements, solid lines are used for the X-FEM results. As expected, it is observed that the overall response is not depending on the modeling technique for the material interface. A small difference in slope of the softening branch is found with increasing difference in stiffness between the two layers. This is related to the way the equivalent traction is defined in the discrete model, namely as the normal component of the effective traction vector. In the interface element, damage evolution is governed by the norm of the displacement jump vector (normal and tangential). In the presence of shear (or a tangential jump) along the interface, damage will grow faster in the interface formulation. The importance of the shear contribution increases with increasing difference in stiffness between both layers. The good agreement between the response of the proposed cohesive zone model and of classical interface elements indicates that the introduction of the approximation for the local stress tensor at zero damage (Eq. 36) is justified.

6 Conclusions

A general strategy to model the mechanical behavior of quasi-brittle materials is proposed. The proposed discrete constitutive equation allows for a smooth transition between the continuum state and the discrete state and ensures equilibrium between the effective tractions in the undamaged material bonds and the stresses in the continuum at every stage of the failure process. The discrete equation can be used in combination with any continuum constitutive model, yielding a continuous-discontinuous material model that can describe the entire failure process. Using a linear elastic continuum model it was shown that, a mesh objective response is obtained. Besides the study of fracture processes in bulk material, the discrete model can also be applied to examine delamination or interface failure. In contrast with classical interface elements, no dummy stiffness is required.

The predictive capabilities of the model crucially depend on the characteristics of the continuum model and the appropriate choice of the damage criterion. It was shown that for mode I, realistic results and trends can already be obtained based on a simple mechanical model (linear elasticity) and failure criterion (Rankine). Extension to other models and failure criteria can be done in an analogue way.

7 Acknowledgements

Funding for this work was provided by the Flemish institute for Science and Technology (IWT-SBO project IT300175).

8 References

[1] G.I. Barenblatt, *The mathematical theory of equilibrium cracks in brittle fracture*, Advances in applied mechanics 7 (1962) p. 55-129.

[2] T. Belytschko and T. Black, *Elastic crack growth in finite elements with minimal remeshing*, Internat. J. Numer. Methods Engrg. 45 (1999) p. 601-620.

[3] G.T. Camacho and M. Ortiz, *Computational modeling of impact damage in brittle materials*, Internat. J. Solids Structures 33 (1996) p. 2899-2938.

[4] J. Dolbow, N. Moës and T. Belytschko, *Discontinuous enrichment in finite elements with a partition of unity method*, Finite Elem. Anal. Des. 36 (2000) p. 235-260.

[5] C.A. Duarte and J.T. Oden, *H-p clouds - an h-p meshless method*, Numer. Methods Partial Differential Equations 12 (1996) p. 673-705.

[6] D.S. Dugdale, *Yielding of steel sheets containing slits*, J. Mech. Phys. Solids 8 (1960) p. 100-104.

[7] M. Jirásek, *Embedded crack models for concrete fracture*, in *EURO-C 1998 Computer modeling of concrete structures*, R. de Borst, N. Bicanic, H. Mang and G. Meschke, eds., Balkema, Rotterdam, 1998.

[8] M. Jirásek and T. Zimmermann, *Embedded crack model. Part II: Combination with smeared cracks*, Internat. J. Numer. Methods Engrg. 50 (2001) p. 1291-1305.

[9] J. Lemaitre, *A continuous damage mechanics model for ductile fracture*, J. Engrg. Mater. and Technol. 107 (1985) p. 83-87.

[10] N. Moës, J. Dolbow and T. Belytschko, *A finite element method for crack growth without remeshing*, Internat. J. Numer. Methods Engrg. 46 (1999) p. 131-150.

[11] J. Oliver, *On the discrete constitutive models induced by strong discontinuity kinematics and continuum constitutive equations*, Internat. J. Solids Structures 37 (2000) p. 7207-7229.

[12] J. Oliver, A.E. Huespe, M.D.G. Pulido and E. Chaves, *From continuum mechanics to fracture mechanics: the strong discontinuity approach*, Engrg. Fracture Mech. 69 (2002) p. 113-136.

[13] K.D. Papoulia, C.-H. Sam and S.A. Vavasis, *Time continuity in cohesive finite element modeling*, Internat. J. Numer. Methods Engrg. 58 (2003) p. 679-701.

[14] Z. Ren and N. Bićanić, *Simulation of progressive fracturing under dynamic loading conditions*, Comm. Numer. Methods Engrg. 13 (1997) p. 127-138.

[15] J.C. Simo and J.W. Ju, *Strain- and stress-based continuum damage models – 1. Formulation*, Internat. J. Solids Structures 23 (1987) 821-840.

[16] A. Simone, G.N. Wells and L.J. Sluys, *From continuous to discontinuous failure in a gradient-enhanced continuum damage model*, Comput. Methods Appl. Mech. Engrg. 192 (2003) p. 4581-4607.

[17] G.N. Wells and L.J. Sluys, *A new method for modelling cohesive cracks using finite elements*, Internat. J. Numer. Methods Engrg. 50 (2001) p. 2667-2682.

	E [GPa]	f_t^0 [MPa]	f_t^1 [MPa]	n [-]	G_f^I [N/m]
(a)	**2.0**	3.0	3.0	1.0	2250.0
	5.0	3.0	3.0	1.0	900.0
	10.0	3.0	3.0	1.0	450.0
	20.0	3.0	3.0	1.0	225.0
	50.0	3.0	3.0	1.0	90.0
(b)	10.0	**2.0**	2.0	1.0	200.0
	10.0	**2.5**	2.5	1.0	312.5
	10.0	**3.0**	3.0	1.0	450.0
	10.0	**3.5**	3.5	1.0	612.5
	10.0	**4.0**	4.0	1.0	800.0
(c)	10.0	3.0	**1.5**	1.0	262.5
	10.0	3.0	**3.0**	1.0	450.0
	10.0	3.0	**4.5**	1.0	712.5
	10.0	3.0	**6.0**	1.0	1050.0
	10.0	3.0	**7.5**	1.0	1462.5
(d)	10.0	3.0	4.5	**0.2**	905.4
	10.0	3.0	4.5	**0.5**	806.3
	10.0	3.0	4.5	**1.0**	712.5
	10.0	3.0	4.5	**2.0**	622.5
	10.0	3.0	4.5	**5.0**	535.2

Table 1: Investigated parameter combinations and resulting fracture energy (according to Eq. 15) for the uniaxial tensile test. Tests are subdivided in four groups (a-d). Corresponding results are shown in Figure 5a-d.

FIGURE CAPTIONS

Figure 1: Schematic representation of (a) an infinitesimal part of a plane with normal **n** in a structure or structural component, (b) the cohesive zone with approximately 60% in-plane micro-damage and (c) the relation between damage, effective tractions and continuum stresses.

Figure 2: Schematic representation of (a) the components of the traction vector as a function of damage and (b) displacement jump. Tractions are indicated with a solid line, effective tractions with a dotted line and the continuum part of the traction with a dashed line.

Figure 3: (a) Body Ω crossed by a displacement discontinuity. (b) Schematic representation of the displacement field and (c) the corresponding strain field of a crossed 1D element.

Figure 4: Uniaxial tensile test: geometry, mesh and boundary conditions.

Figure 5: Uniaxial tensile test: sensitivity analysis of (a) Youngs modulus, (b) tensile strength, (c) residual tensile strength and (d) hardening exponent. All parameter combinations are listed in **Error! Reference source not found.**.

Figure 6: 4pt-bending test: geometry, meshes and boundary conditions.

Figure 7: 4pt-bending test: load-displacement curves obtained with meshes based on (a) Q4 and (b) T3 elements.

Figure 8: Double cantilever beam: geometry, mesh and boundary conditions.

Figure 9: Double cantilever beam: load-displacement curves for various material combinations as obtained with the cohesive zone model (solid line) and interface elements (dashed line).

FIGURE 1

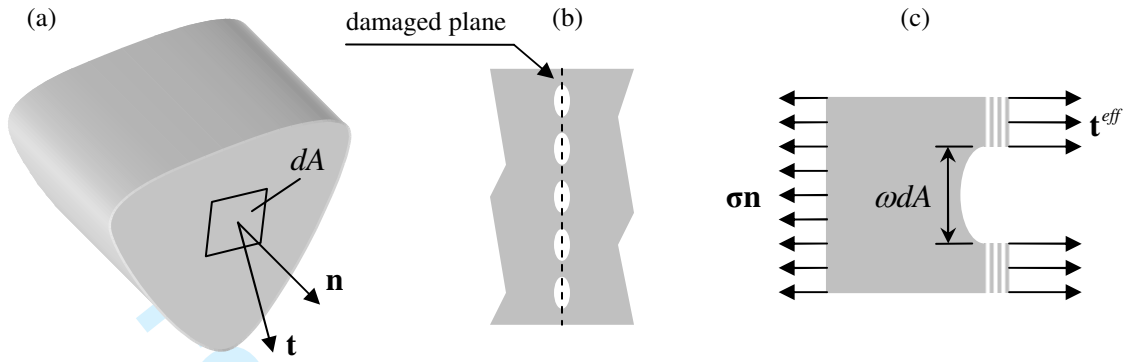

FIGURE 2

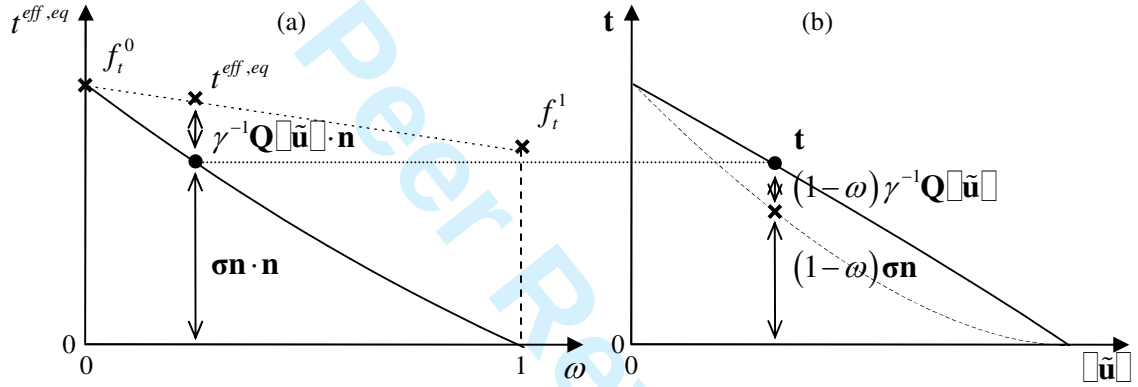

FIGURE 3

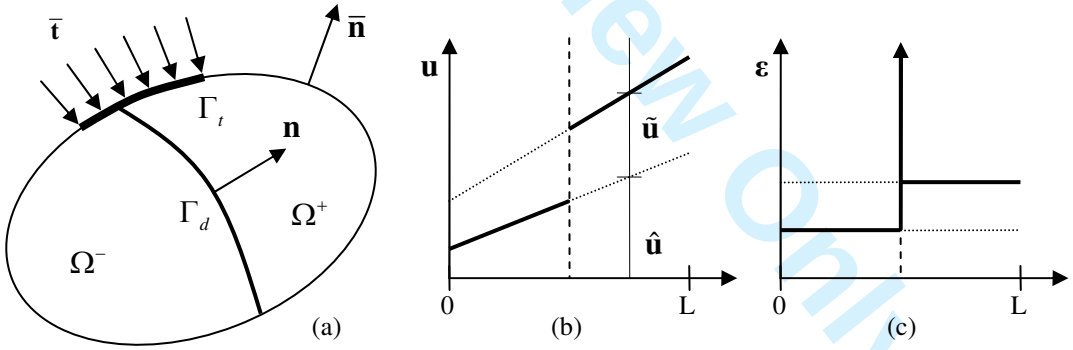

FIGURE 4

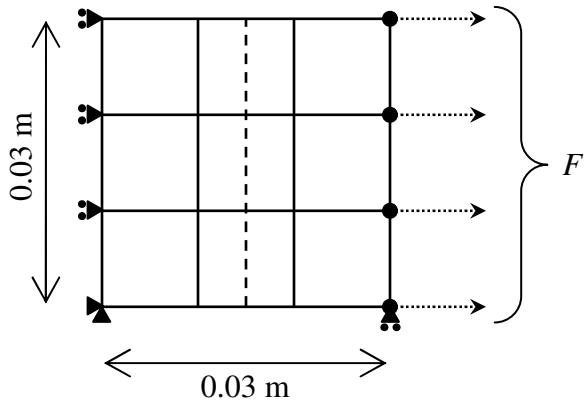

FIGURE 5

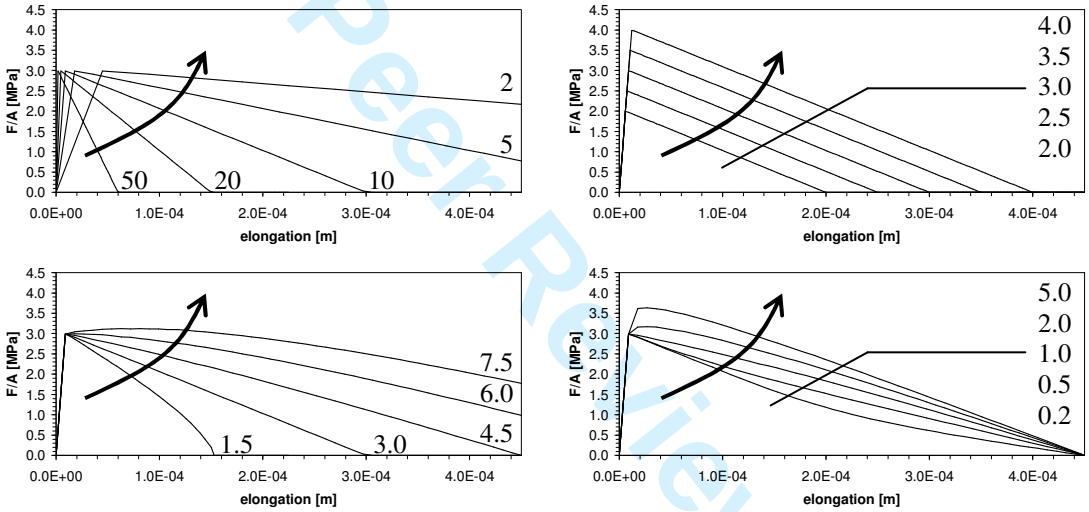

FIGURE 6

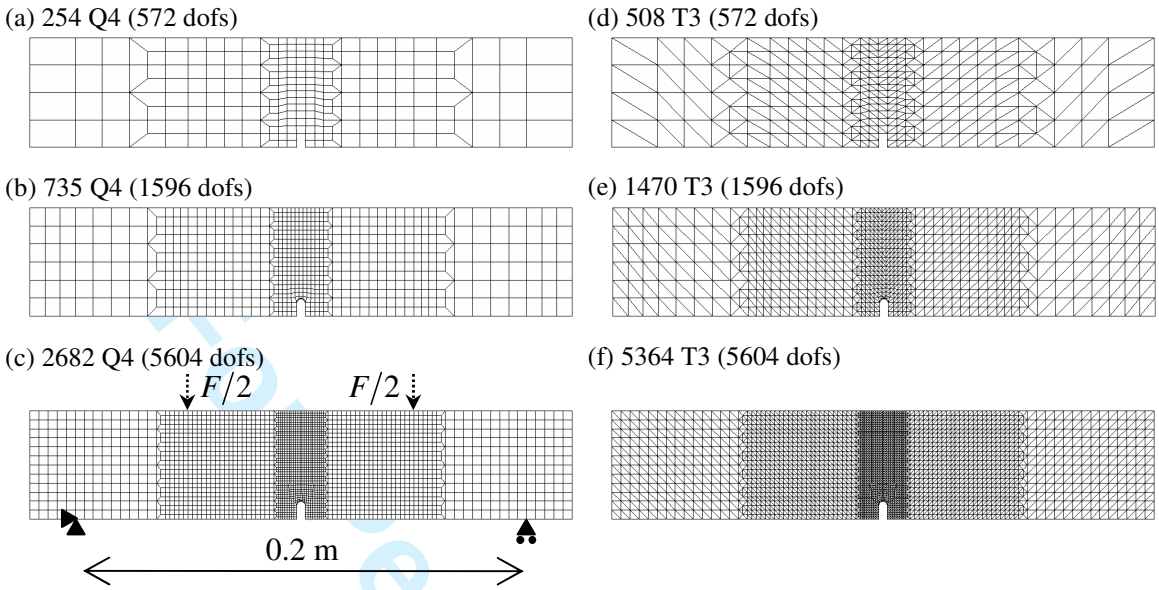

FIGURE 7

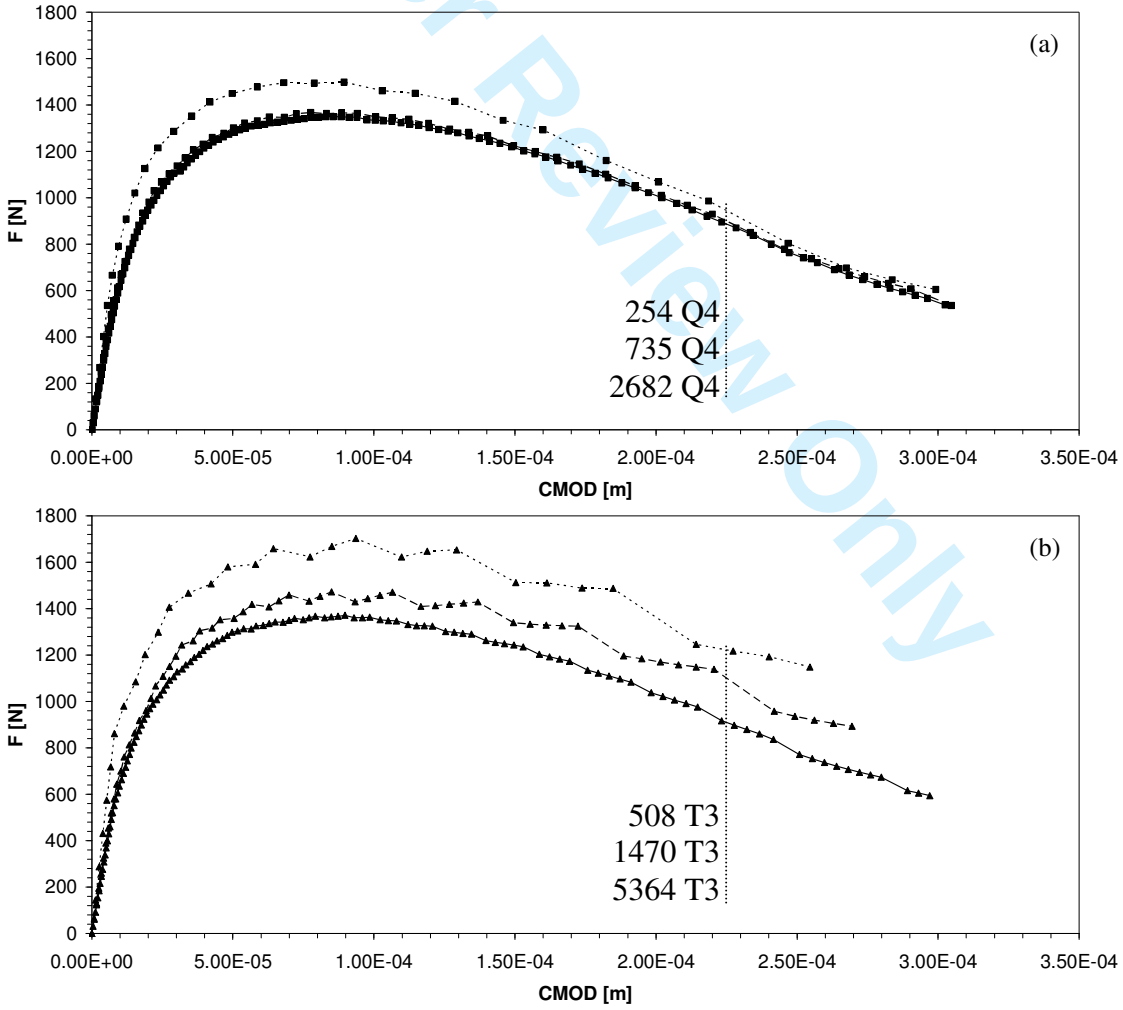

FIGURE 8

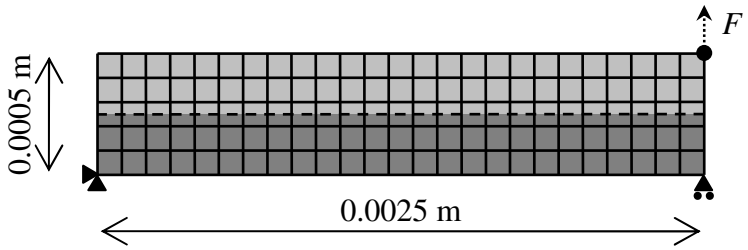

FIGURE 9

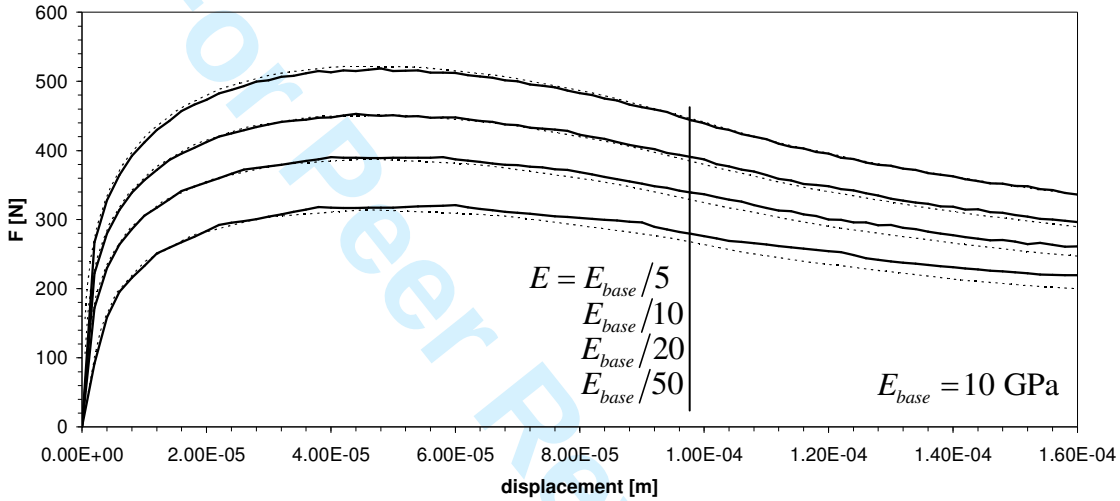

A continuous-discontinuous approach to simulate fracture processes in quasi-brittle materials

P. Moonen[(1,2)], J. Carmeliet[(3,4)], L.J. Sluys[(1)]

(1) Department of Civil Engineering and Geosciences, Delft University of Technology, Stevinweg 1, 2628 CN Delft, The Netherlands
(2) Laboratory of Building Physics, Department of Civil Engineering, Katholieke Universiteit Leuven, Kasteelpark Arenberg 40, 3001 Leuven, Belgium
(3) Institute for Building Technology, Department of Architecture, Swiss Federal Institute of Technology Zürich (ETH), Wolfgang-Pauli-Str. 15, 8093 Zürich, Switzerland
(4) Laboratory for Building Technologies, Swiss Federal Laboratories for Materials Testing and Research (EMPA), Überlandstrasse 129, 8600 Dübendorf, Switzerland

1 Abstract

A macroscopic framework for the simulation of failure processes in quasi-brittle materials is proposed. The framework employs the partition of unity (PU) concept and introduces a new cohesive zone model, capturing the transition between the initial continuum state and the final discrete state. The model is generic in a sense that it allows extending most continuum models to a discontinuous framework in an efficient and robust way, hereby adding the effect of macro-crack formation by the growth and coalescence of micro-defects. Both material failure and interface failure can be studied with this formulation.

Keywords: fracture, cohesive zone model, X-FEM, continuous-discontinuous framework.

2 Introduction

In the past decades, significant progress has been made in computational modeling of damage and fracture processes in quasi-brittle materials such as concrete and masonry. Most of the available models are continuum models which require very fine finite element meshes in the vicinity of a crack or localization zone. Discrete models are consistent with the physical observation of a discrete crack as a displacement jump across a discontinuity surface. The extended finite element approach belongs to this class of models (see, for example, [2,4,10,17]). In this formulation, cracks are not restricted to the finite element boundaries; instead, they can freely run through the finite element mesh. As a result, coarser meshes can be used, rendering these models suitable for larger scale computations. However, an embedded discontinuity in a coarse mesh cannot accurately represent the energy consumed by micro-crack branching prior to the formation of the macro-crack. A better characterization of the whole failure process can be achieved by combining continuous and discontinuous theories into a global macroscopic framework.
This idea has been successfully pursued by many authors (see, for example, [8,12,14,16]), nevertheless some issues remain. It is for example not clear when a discrete

crack should be introduced. Some authors introduce a traction-free discontinuity at the final stages of failure. In this case the continuum model governs the softening behavior (see, for example, [16]). Other authors make use of the cohesive zone assumption (see [1,6]). Here a traction-separation model governs the non-linear behavior in the fracture process zone and the continuum can remain elastic at all times (see, for example, [17]). Both approaches have in common that a single moment exists at which the continuum model is replaced by a discrete model. The distinct feature of the model proposed in the present paper is that this transition takes place gradually. A damage-type cohesive law allows using the constitutive model for the continuum in the undamaged material bonds at the process zone, whereas the damaged part of the crack is traction-free. As damage grows, material bonds are broken and a macro-crack is formed. This conceptually different cohesive zone model is formulated irrespective of the underlying model for the undamaged material. The gradual transition ensures that the stress at a point varies in a continuous manner during the entire solution trajectory. This concept is known as 'time continuity', and was introduced by Papoulia et al. [13] as a prerequisite for robustness of a continuous-discontinuous framework.

The paper starts by introducing the discrete constitutive equations (Section 3.1) and the continuum material model (Section 3.2). The implementation in a strong discontinuity framework is discussed in section 4. In section 5 several aspects of the model are highlighted by means of numerical examples.

3 Constitutive equations

3.1 Discrete constitutive model

3.1.1 Damage-based discrete constitutive equation

Consider an infinitesimal part of a plane dA with unit normal $\mathbf{n}$ in a structure or structural component (Figure 1a). The tractions $\mathbf{t}$ acting on this plane are obtained as

$$\mathbf{t} = \boldsymbol{\sigma}\mathbf{n} \tag{1}$$

where $\boldsymbol{\sigma}$ is the second order continuum stress tensor. Tensile tractions have a positive sign. Suppose that micro-cracks and -voids start to grow on this infinitesimal plane (Figure 1b). In that case, we can quantify the ratio between the damaged area and the total area with a scalar damage variable ω, ranging from zero to one. Zero damage corresponds to the undamaged bulk material, whereas ω equals one upon complete separation along the crack plane. The bulk material will, in general, include pores, deficiencies and irregularities. All these 'imperfections' are randomly distributed in the material. As a result, they are not considered as 'damage' but rather as a characteristic of the continuum.

Tractions can only be transferred in the material through the undamaged material bonds. We assumed that the micro-voids and -cracks influence the stress field in the surrounding continuum material only locally. If the micro-voids and -cracks grow and coalesce into macro-cracks, the surrounding material will relax and all stresses will vanish. Hence, it is reasonable to assume that the effective tractions in the material bonds $\mathbf{t}^{eff}$, acting on the undamaged part of the infinitesimal area dA, equal the homogenized stresses in the

surrounding continuum, projected on the plane and acting on the same area (Figure 1c), or

$$\boldsymbol{\sigma}\mathbf{n}\,dA = \mathbf{t}^{eff}\left(1-\omega\right)dA \;\text{ for }\; 0 \le \omega \le 1 \tag{2}$$

Before any damage occurs, the effective tractions equal the continuum stresses (Eq. 2 with $\omega = 0$). As damage grows, the active area decreases and higher effective tractions are needed to maintain equilibrium with the continuum stresses. The redistribution of the tractions causes additional deformations in the undamaged material bonds. Therefore, the effective traction can be additively decomposed into two terms, namely, (i) the initial traction prior to damage growth and (ii) the traction related to the damage-induced elongation of the material bond:

$$\mathbf{t}^{eff} = \boldsymbol{\sigma}\mathbf{n} + \gamma^{-1}\mathbf{Q}\left[\!\left[\tilde{\mathbf{u}}\right]\!\right] \tag{3}$$

where $\mathbf{Q} = \mathbf{nDn}$ is the acoustic tensor, with $\mathbf{D}$ a 4th order constitutive tensor describing the constitutive behavior of the bulk material, $\left[\!\left[\tilde{\mathbf{u}}\right]\!\right]$ is a displacement jump corresponding to the elongation of the material bond, γ is one unit length and follows from dimensional analysis. The acoustic tensor represents the projection of the bulk behavior onto the discontinuity plane. If the discontinuity plane corresponds to a material interface, we can either use the acoustic tensor of the bond material (i.e. the glue) or - in absence of a bonding material - the acoustic tensor of the coupled system:

$$\mathbf{Q} = 2\left(\mathbf{Q}_1^{-1} + \mathbf{Q}_2^{-1}\right)^{-1} \tag{4}$$

where $\mathbf{Q}_1$ and $\mathbf{Q}_2$ represent the acoustic tensors of both materials. The latter choice implies a perfect bond between both. In case of two equal materials $\mathbf{Q} = \mathbf{Q}_1 = \mathbf{Q}_2$.

Combining equations (1-3) finally yields the constitutive equation for the cohesive zone:

$$\mathbf{t} = \left(1-\omega\right)\left[\boldsymbol{\sigma}\mathbf{n} + \gamma^{-1}\mathbf{Q}\left[\!\left[\tilde{\mathbf{u}}\right]\!\right]\right] \tag{5}$$

Equation (5) represents the gradual degradation from a continuum to a discrete state. Figure 2 illustrates this equation in a graphical way for a one dimensional case with a specific choice of the model parameters. Upon initiation of the crack, the crack width and the damage variable equal zero and equation (1) is recovered: the material behaves as if no discontinuity were present. As damage grows, the relative contribution of the discrete component of the total traction gains importance over the continuum component (Figure 2b, dashed line). At rupture, the damage variable becomes one and the traction forces become zero. This corresponds to a traction-free discontinuity.

If the loading were reversed before rupture occurred, the damage would cease to grow, but equation (5) can still be used without modification to obtain the total traction vector. As the stress decreases, both crack width and total traction will decrease, and finally become zero.

3.1.2 Damage evolution

The proposed discrete constitutive equation needs to be supplemented with a proper damage criterion and a suitable damage evolution law.

Criteria for damage growth are either stress-based or strain-based. In a discrete setting, the corresponding criteria are traction-based or displacement jump-based. Considering that (i) the discrete law (Eq. 5) depends on the equilibrium between the effective tractions in the undamaged material bonds and the homogenized stresses in the surrounding

continuum matrix, and that (ii) the corresponding strain field is unbounded if localization occurs in a band of zero width, it is clear that a traction-based damage criterion is preferred in this formulation. In this study, a rankine-type damage criterion is adopted:

$$f\left(\mathbf{t}^{eff},\omega\right)=t^{eff,eq}-\kappa\leq 0 \tag{6}$$

in which $t^{eff,eq}\left(\mathbf{t}^{eff}\right)$ is an equivalent traction, expressed as a function of the effective tractions, and $\kappa(\omega)$ is the residual strength of the damaged material. For mode I dominated failure, the following expression for the equivalent traction is found suitable:

$$t^{eff,eq}=\mathbf{t}^{eff}\cdot\mathbf{n} \tag{7}$$

A simple, yet flexible, expression for κ is given by

$$\kappa(\omega)=f_t^0+\left(f_t^1-f_t^0\right)\omega^n \tag{8}$$

with $f_t^0>0$ the tensile strength of the virgin bulk material, $f_t^1\geq 0$ the residual tensile strength of the damaged bulk material, and $n\geq 0$ a hardening/softening exponent.

The damage evolution law is defined by the Kuhn-Tucker conditions:

$$\dot{\omega}\geq 0,\ f\leq 0,\ \dot{\omega}f=0 \tag{9}$$

supplemented with the consistency condition:

$$\dot{\omega}\dot{f}=0 \tag{10}$$

The damage evolution law is not explicitly given in terms of e.g. the equivalent traction. The updated values of the damage and the corresponding traction vector and crack width are obtained via return mapping, similar to plasticity. This algorithm will be discussed in more detail in section 4.7.

3.1.3 *Determination of the mode I fracture energy*

The fracture energy is defined as:

$$G_f=\int_0^{+\infty}\mathbf{t}\cdot d[\![\tilde{\mathbf{u}}]\!] \tag{11}$$

Upon crack propagation, the traction can be expressed as:

$$\mathbf{t}=(1-\omega)\mathbf{t}^{eff}=(1-\omega)\kappa\frac{\mathbf{m}}{\mathbf{m}\cdot\mathbf{n}} \tag{12}$$

where $\mathbf{m}$ is a unit vector pointing in the direction of the displacement jump. The form of equation (12) is closely related to the expression for the equivalent effective traction (Eq. 7) and accordingly does not hold for pure mode II loading ($\mathbf{m}\cdot\mathbf{n}=0$).

The displacement jump can be expressed as:

$$[\![\tilde{\mathbf{u}}]\!]=\omega\kappa\gamma\mathbf{Q}^{-1}\frac{\mathbf{m}}{\mathbf{m}\cdot\mathbf{n}} \tag{13}$$

Equation (13) is derived from (5), after eliminating $\boldsymbol{\sigma}\mathbf{n}$ by means of (1) and $\mathbf{t}$ by means of (12). Substituting equations (12) and (13) in (11) and taking into account that for pure mode I loading $\mathbf{m}=\mathbf{n}$, we obtain the mode I fracture energy G_f^I:

$$\begin{aligned}G_f^I&=\int_0^1(1-\omega)\kappa\mathbf{n}\cdot\left(\omega\frac{\partial\kappa}{\partial\omega}+\kappa\right)\gamma\mathbf{Q}^{-1}\mathbf{n}d\omega\\&=\left(\mathbf{n}\cdot\mathbf{Q}^{-1}\mathbf{n}\right)\gamma\int_0^1(1-\omega)\left(\omega\frac{\partial\kappa}{\partial\omega}+\kappa\right)\kappa d\omega\end{aligned} \tag{14}$$

If κ is defined according to equation (8) the expression becomes:

$$G_f^I = \left(\mathbf{n}\cdot\mathbf{Q}^{-1}\mathbf{n}\right)\gamma\frac{\left(2n^2\left(f_t^0\right)^2+2nf_t^0f_t^1+(n+1)\left(f_t^1\right)^2\right)}{2(n+1)(2n+1)} \tag{15}$$

In the special case that $f_t^1 = f_t^0 = f_t$, this expression reduces to $G_f^I = \left(\mathbf{n}\cdot\mathbf{Q}^{-1}\mathbf{n}\right)\gamma\frac{1}{2}f_t^2 = \frac{1}{2}\left(\left[\!\left[\tilde{\mathbf{u}}_{\max}\right]\!\right]\cdot\mathbf{n}\right)f_t$, which corresponds to the classical case of linear softening in e.g. interface elements. $\left[\!\left[\tilde{\mathbf{u}}_{\max}\right]\!\right]$ is obtained from equation (13) with $\omega = 1$. Note that no softening parameter (n) is required in case $f_t^1 = f_t^0 = f_t$.

3.1.4 Crack initiation and propagation

Finally, we need to define when a discontinuity should initiate or propagate. We have already shown that upon crack initiation, the discrete constitutive equation (Eq. 5) reduces to traction equilibrium on the potential crack plane (Eq. 1). In the same line of reasoning, the discrete damage criterion (Eq. 6) corresponds to the following initiation criterion:

$$f = \sigma_i - \kappa^0 \le 0 \tag{16}$$

with σ_i the i$^{\text{th}}$ principal stress and $\kappa^0 = \kappa(\omega = 0)$. If equation (16) is violated at a material point, a new crack segment is introduced with the normal pointing in the (critical) principal stress direction.

It is recommended to determine the direction of the discontinuity based on the non-local stress tensor $\bar{\boldsymbol{\sigma}}$, calculated as a weighted average of stresses using a Gaussian weighting function w (see [7]):

$$\bar{\boldsymbol{\sigma}} = \frac{\int_\Omega w\boldsymbol{\sigma}d\Omega}{\int_\Omega w d\Omega} \text{ with } w = \frac{1}{(2\pi)^{3/2}l^3}\exp\left(-\frac{r^2}{2l^2}\right) \tag{17}$$

where r is the distance to the crack tip and l the influence length, taken approximately equal to three times the element size (see [17]).

3.2 Continuum constitutive model

The framework has been formulated irrespective of the constitutive model used for the continuum. To avoid confusion between softening behavior caused by either the continuum or the discrete constitutive model, we use a linear elastic bulk model according to:

$$\boldsymbol{\sigma} = \mathbf{D}\boldsymbol{\varepsilon} \tag{18}$$

with $\mathbf{D} = \lambda\mathbf{1}\otimes\mathbf{1} + 2\mu\mathbf{I}$ the elasticity tensor, $\mathbf{1}$ and $\mathbf{I}$ the second and fourth order unit tensors, and λ and μ the lamé constants. $\boldsymbol{\varepsilon}$ is the second order strain tensor. The softening response is thus due to the discrete constitutive model.

4 Implementation in a strong discontinuity framework

4.1 Kinematics

Figure 3a illustrates a body Ω crossed by a displacement discontinuity Γ_d. Using the PU-concept (see [5]), the total displacement field is given by:

$$\mathbf{u} = \hat{\mathbf{u}} + H_{\Gamma_d}\tilde{\mathbf{u}} \tag{19}$$

where $\hat{\mathbf{u}}$ and $\tilde{\mathbf{u}}$ are smooth, continuous functions on Ω and H_{Γ_d} is the Heaviside step function corresponding to and centered at the discontinuity Γ_d (Figure 3b). The Heaviside function is equal to one for all points $x \in \Omega^+$ and zero for all other points $x \in \Omega^-$.

The total strain field $\boldsymbol{\varepsilon}^{tot}$ (Figure 3c) can be found by taking the symmetric gradient of the displacement field:

$$\boldsymbol{\varepsilon}^{tot} = \nabla^s \mathbf{u} = \nabla^s \hat{\mathbf{u}} + H_{\Gamma_d}\nabla^s \tilde{\mathbf{u}} + \delta_{\Gamma_d}\left(\tilde{\mathbf{u}} \otimes \mathbf{n}\right)^s \tag{20}$$

where $\mathbf{n}$ is the normal to the discontinuity and δ_{Γ_d} is the Dirac delta distribution, centered at the discontinuity. The Dirac delta distribution is the derivative of the Heaviside step function and is nonzero only for the points on the discontinuity.

4.2 Strong form

The equilibrium equation in absence of body forces reads:

$$\nabla \cdot \boldsymbol{\sigma} = 0 \text{ in } \Omega \tag{21}$$

The natural boundary conditions are given by:

$$\boldsymbol{\sigma}\bar{\mathbf{n}} = \bar{\mathbf{t}} \text{ on } \Gamma_t \tag{22a}$$

$$\boldsymbol{\sigma}\mathbf{n} = -\mathbf{t}_d^+ \text{ on } \Gamma_d^+ \tag{22b}$$

$$\boldsymbol{\sigma}\mathbf{n} = \mathbf{t}_d^- \text{ on } \Gamma_d^- \tag{22c}$$

where $\boldsymbol{\sigma}$ is the second order stress tensor, $\bar{\mathbf{n}}$ is the outward normal to the body, $\mathbf{n}$ is the outward normal to Ω^- on Γ_d^-. The minus sign indicates that the direction of the tractions $\mathbf{t}_d^+$ is opposite to the direction of $\mathbf{n}$. Tensile tractions are taken positive.

The essential boundary conditions are:

$$\mathbf{u} = \bar{\mathbf{u}} \text{ on } \Gamma_u \tag{23}$$

4.3 Weak form

Weak equilibrium statement is written as:

$$\int_\Omega \mathbf{w} \cdot \left(\nabla \cdot \boldsymbol{\sigma}\right) d\Omega = 0 \tag{24}$$

Which must hold for all admissible variations of displacement $\mathbf{w}$. Following a Galerkin approach (i.e. taking the space of admissible variations the same as the actual displacements) leads, after standard manipulations, to the following set of variational statements:

$$\int_\Omega \nabla^s \hat{\mathbf{w}} : \boldsymbol{\sigma} d\Omega = \int_{\Gamma_d^-} \hat{\mathbf{w}} \cdot \mathbf{t}_d^- d\Gamma + \int_{\Gamma_d^+} \hat{\mathbf{w}} \cdot \mathbf{t}_d^+ d\Gamma + \int_{\Gamma_t} \hat{\mathbf{w}} \cdot \bar{\mathbf{t}} d\Gamma \tag{25a}$$

$$\int_\Omega H_{\Gamma_d} \nabla^s \tilde{\mathbf{w}} : \boldsymbol{\sigma} d\Omega = \int_{\Gamma_d^-} H_{\Gamma_d}^- \tilde{\mathbf{w}} \cdot \mathbf{t}_d^- d\Gamma + \int_{\Gamma_d^+} H_{\Gamma_d}^+ \tilde{\mathbf{w}} \cdot \mathbf{t}_d^+ d\Gamma + \int_{\Gamma_t} H_{\Gamma_d} \tilde{\mathbf{w}} \cdot \bar{\mathbf{t}} d\Gamma \quad (25b)$$

4.4 Discretized form

Nodes whose support is crossed by a discontinuity are assigned a regular and an enhanced set of degrees of freedom, denoted with $\mathbf{a}$ and $\mathbf{b}$, respectively. The discretized format of equation (19) then reads:

$$\mathbf{u} = \mathbf{N}\mathbf{a} + H_{\Gamma_d} \mathbf{N}\mathbf{b} \quad (26)$$

Where $\mathbf{N}$ is the array containing the finite element shape functions. The strain field can be discretized in a similar fashion using the interpolation matrix $\mathbf{B}$. For elements with only regular degrees of freedom $\mathbf{a}$, the problem fields are discretized in the standard way.

The discretized format of the weak governing equations reads:

$$\int_\Omega \mathbf{B}^T \boldsymbol{\sigma} d\Omega = \int_{\Gamma_t} \mathbf{N}^T \bar{\mathbf{t}} d\Gamma \quad (27a)$$

$$\int_\Omega H_{\Gamma_d} \mathbf{B}^T \boldsymbol{\sigma} d\Omega = \int_{\Gamma_d^+} H_{\Gamma_d}^+ \mathbf{N}^T \mathbf{t}_d^+ d\Gamma + \int_{\Gamma_t} H_{\Gamma_d} \mathbf{N}^T \bar{\mathbf{t}} d\Gamma \quad (27b)$$

where we used the relations $\mathbf{t}_d^+ = -\mathbf{t}_d^-$ and $H_{\Gamma_d}^- = 0$.

4.5 Discretization of the constitutive relations

The stress in the bulk material (see Eq. 18) is expressed in terms of the nodal displacements as:

$$\boldsymbol{\sigma} = \mathbf{D}\boldsymbol{\varepsilon} = \mathbf{D}\left(\mathbf{B}\mathbf{a} + H_{\Gamma_d} \mathbf{B}\mathbf{b}\right) \quad (28)$$

If the shape functions were able to exactly represent the displacement field, the true stress tensor could be computed by means of equation (28). In practice, the interpolation functions are a limited subset of the entire solution space, and equation (28) provides only an approximate value for the local stress tensor at a point. However, the proposed discrete model, as described in Section 3.1, relies on the knowledge of the true local stress tensor to ensure a gradual transition from a continuum to a discrete state. Simply inserting the discretized expressions for displacement and stress in equation (5) could lead to inaccurate results, especially in the study of dynamic problems or in case a non-linear constitutive model for the bulk material is used. By casting the discrete traction law in a different format prior to discretization, the successful use of the method is no longer restricted to linear elastic, quasi-static simulations.

We first make a distinction between two types of transitions: namely (i) the transition to strong discontinuity kinematics (i.e. the insertion of a discontinuity in the displacement field) and (ii) the transition from a continuous to a discontinuous state as described by the cohesive model. The former corresponds to the moment at which the propagation criterium (Eq. 16) at a point is violated and a strong discontinuity is inserted with zero damage ($\omega = 0$); the latter relates to the process of damage evolution ($0 < \omega \leq 1$).

4.5.1 Transition to strong discontinuity kinematics

From equation (13) it is clear that a jump in the displacement field cannot exist in absence of damage ($\omega = 0$). The use of strong discontinuity kinematics (with a Heaviside enrichment) is therefore not required. However, the displacement field does not need to

be smooth, hence the strain field can exhibit a jump across the discontinuity, as long as equilibrium is satisfied:

$$\llbracket \boldsymbol{\sigma} \rrbracket \mathbf{n} = \mathbf{0} \tag{29}$$

A discontinuity in the strain field is termed a weak discontinuity. In the corresponding description of the displacement field, the distance function is usually used as enrichment function. In contrast with strong discontinuity kinematics, weak discontinuity kinematics does not give rise to integrals over the discontinuity in the weak form. Hence it is not needed to provide an explicit expression for the cohesive traction if $\omega = 0$.

4.5.2 *Transition from a continuous to a discontinuous state*

Since the damage variable is nonzero during the transition, we can eliminate the continuum stress from equation (5) by means of equation (1):

$$\mathbf{t} = \left(\frac{1-\omega}{\gamma \omega} \right) \mathbf{Q} \llbracket \tilde{\mathbf{u}} \rrbracket \text{ with } 0 < \omega \leq 1 \tag{30}$$

This expression allows computing the traction vector solely based on the displacement jump. The dependency on the continuum stress tensor is implicitly present.

At this point, it is worthwhile to make a comparison with another cohesive law used in a strong discontinuity context. Therefore, we substitute the damage variable by $\omega = \left(1 + \gamma \left(1 - \varpi\right)\right)^{-1}$:

$$\mathbf{t} = \left(1 - \varpi\right) \mathbf{Q} \llbracket \tilde{\mathbf{u}} \rrbracket \text{ with } -\infty < \varpi \leq 1 \text{ m}^{-1} \tag{31}$$

Equation (31) has been obtained by Oliver [11], by performing a strong discontinuity analysis of the isotropic damage model of Simo [15]. As compared to our formulation, two important differences have to be noted: (i) the dimensional damage variable ϖ ranging from $-\infty$ m^{-1} to one m^{-1} is physically less relevant than the dimensionless variable ω ranging from zero to one, and (ii) the singularity at $\omega = 0$ (in Eq. 30) arises from an attempt to avoid errors introduced by the discretization, whereas the singularity at $\varpi = -\infty$ m^{-1} (in [11]) results from the presence of a Dirac delta distribution in the strain field for strong discontinuity kinematics.

4.6 Linearized and discretized form

After linearization, the system of equations becomes:

$$\begin{bmatrix} \mathbf{K}_{aa}^{i} & \mathbf{K}_{ab}^{i} \\ \mathbf{K}_{ba}^{i} & \mathbf{K}_{bb}^{i} \end{bmatrix} \begin{bmatrix} \delta \mathbf{a}^{i+1} \\ \delta \mathbf{b}^{i+1} \end{bmatrix} = \begin{bmatrix} \mathbf{f}_{ext,a}^{i} \\ \mathbf{f}_{ext,b}^{i} \end{bmatrix} - \begin{bmatrix} \mathbf{f}_{int,a}^{i} \\ \mathbf{f}_{int,b}^{i} \end{bmatrix} \tag{32}$$

With

$$\mathbf{K}_{aa} = \int_{\Omega} \mathbf{B}^{T} \mathbf{D} \mathbf{B} d\Omega \tag{33a}$$

$$\mathbf{K}_{ba} = \mathbf{K}_{ab}^{T} = \int_{\Omega} H_{\Gamma_d} \mathbf{B}^{T} \mathbf{D} \mathbf{B} d\Omega \tag{33b}$$

$$\mathbf{K}_{bb} = \int_{\Omega} H_{\Gamma_d} \mathbf{B}^{T} \mathbf{D} \mathbf{B} d\Omega + \int_{\Gamma_d^{+}} H_{\Gamma_d} \mathbf{N}^{T} \mathbf{T}^{+} \mathbf{N} d\Gamma \tag{33c}$$

$$\mathbf{f}_{ext,a} = \int_{\Gamma_t} \mathbf{N}^{T} \bar{\mathbf{t}} d\Gamma \tag{33d}$$

$$\mathbf{f}_{ext,b} = \int_{\Gamma_t} H_{\Gamma_d} \mathbf{N}^{T} \bar{\mathbf{t}} d\Gamma \tag{33e}$$

$$\mathbf{f}_{int,a} = \int_{\Omega} \mathbf{B}^T \boldsymbol{\sigma} d\Omega \tag{33f}$$

$$\mathbf{f}_{int,b} = \int_{\Omega} H_{\Gamma_d} \mathbf{B}^T \boldsymbol{\sigma} d\Omega + \int_{\Gamma_d^+} H_{\Gamma_d} \mathbf{N}^T \mathbf{t}^+ d\Gamma \tag{33g}$$

The superscript i indicates the iteration counter in the global iterative procedure. The matrix $\mathbf{T}$ follows from the linearization of the discrete model and is given by:

$$\mathbf{T} = \left(\frac{1-\omega}{\gamma\omega} \right) \mathbf{Q} - \frac{1}{\gamma\omega} \frac{\mathbf{t}^{eff} \otimes \mathbf{n}\mathbf{Q}}{\kappa + \omega \dfrac{\partial \kappa}{\partial \omega}} \quad \text{where } 0 < \omega \leq 1 \tag{34}$$

in the case of loading. For unloading and reloading, the discrete tangent becomes

$$\mathbf{T} = \left(\frac{1-\omega}{\gamma\omega} \right) \mathbf{Q} \quad \text{where } 0 < \omega \leq 1 \tag{35}$$

Although the above derivation is theoretically sound, the use of equations (34) or (35) will have a negative impact on the condition number of the stiffness matrix for very small values of the damage variable. A pragmatic approach is followed. Equations (34) and (35) are used if the damage variable exceeds a predefined threshold ω_{crit}, where ω_{crit} is a real positive number close to zero. Below ω_{crit}, it is more accurate to use the original expression for the discrete law (Eq. 5) where the local stress tensor is approximated as:

$$\boldsymbol{\sigma}^{approx.} = \tfrac{1}{2}\left(\boldsymbol{\sigma}^- + \boldsymbol{\sigma}^+ \right) \tag{36}$$

In equation (36) $\boldsymbol{\sigma}^-$ and $\boldsymbol{\sigma}^+$ are the stress tensors, evaluated at the negative and positive side of the discontinuity. The tangent for $0 \leq \omega < \omega_{crit}$ follows directly from the linearisation of equation (5), and contains contributions to $\mathbf{K}_{ba}$ and $\mathbf{K}_{bb}$. Since the approximated expressions can be used for $\omega = 0$, there is no need to employ weak discontinuity kinematics. The validity of this approximation is verified in Section 5.3.

4.7 Return mapping

First, the system of equations (Eq. 32) is solved using the previous converged value of the damage variable (trial state). Next, the effective traction is computed for each point on the discontinuity and the admissibility of the stress state is verified. If the damage criterion is satisfied, i.e. $f \leq 0$, the stress state is admissible and the trial state is the real state. However, if the damage criterion is violated ($f > 0$), the damage variable needs to be updated.

The new damage variable can be found as the root of the damage criterion (Eq. 6). Generally, κ can be a non-linear function of ω, and an explicitly solving for ω is not possible. Therefore a local iterative scheme should be applied (e.g. Newton-Raphson scheme):

$$f^{j+1} = f^j + \left. \frac{\delta f}{\delta \omega} \right|_{\omega^j} \left(\omega^{j+1} - \omega^j \right) + R^2 \tag{37}$$

Where the superscript j denotes the counter in the local iterative procedure. Omitting the terms of second order and higher and elaborating the derivative yields:

$$f^{j+1} = f^j + \left(\left. \frac{\delta t^{eff,eq}}{\delta \omega} \right|_{\omega^j} - \left. \frac{\delta \kappa}{\delta \omega} \right|_{\omega^j} \right) \left(\omega^{j+1} - \omega^j \right) \tag{38}$$

The term $\frac{\delta\kappa}{\delta\omega}$ represents the change in residual strength of the material bonds during damage evolution, and can be obtained by derivation of equation (8). The term $\frac{\delta t^{eff,eq}}{\delta\omega}$ describes the variation of the effective stresses upon increasing damage. In the proposed discrete model, the evolution of damage is not explicitly given in terms of the equivalent traction. An expression for $\delta t^{eff,eq}$ can be obtained under the assumption that the total strain $\boldsymbol{\varepsilon}_{\Gamma_d}^{tot}$ at the discontinuity remains constant during a global iteration.

In analogy with the additive decomposition of the effective traction vector (see Eq. 3), the strain field at the discontinuity $\boldsymbol{\varepsilon}_{\Gamma_d}^{tot}$ is assumed to consist of two terms, namely, (i) an initial strain prior to the development of a strong discontinuity (i.e. with $[\![\tilde{\mathbf{u}}]\!]=0$) and (ii) a strain-like term related to the displacement jump at the discontinuity:

$$\boldsymbol{\varepsilon}_{\Gamma_d}^{tot} = \boldsymbol{\varepsilon} + \zeta\left([\![\tilde{\mathbf{u}}]\!]\otimes\mathbf{n}\right)^s \tag{39}$$

Comparison with equation (20) points out that $\boldsymbol{\varepsilon}=\nabla^s\hat{\mathbf{u}}+H_{\Gamma_d}\nabla^s\tilde{\mathbf{u}}$ is the 'continuum' strain field and $\zeta\left([\![\tilde{\mathbf{u}}]\!]\otimes\mathbf{n}\right)^s$ with $\zeta=\delta_{\Gamma_d}$ is the 'discrete' contribution. The latter is theoretically unbound due to the presence of the Dirac delta function. In the spirit of strong discontinuity analysis, we consider a discontinuity band of bandwidth h, instead of a discontinuity plane with zero thickness. ζ can than be defined as:

$$\zeta=\begin{cases}0 & \Leftrightarrow x\notin\left[-\frac{1}{2}h,\frac{1}{2}h\right]\\ h^{-1} & \Leftrightarrow x\in\left[-\frac{1}{2}h,\frac{1}{2}h\right]\end{cases} \tag{40}$$

In the limit of $h\to 0$ we have $\zeta=\delta_{\Gamma_d}$. Pre- and post-multiplying equation (39) with the stiffness $\mathbf{D}$ and the normal to the discontinuity $\mathbf{n}$, respectively, leads to:

$$\mathbf{D}\boldsymbol{\varepsilon}_{\Gamma_d}^{tot}\mathbf{n} = \boldsymbol{\sigma}\mathbf{n} + \zeta\mathbf{Q}[\![\tilde{\mathbf{u}}]\!] \tag{41}$$

where we made use of the constitutive equation (Eq. 18) and the definition of the acoustic tensor. Rearranging yields:

$$\mathbf{D}\boldsymbol{\varepsilon}_{\Gamma_d}^{tot}\mathbf{n} = \left(1-\zeta\gamma\right)\boldsymbol{\sigma}\mathbf{n} + \zeta\gamma\left(\boldsymbol{\sigma}\mathbf{n}+\gamma^{-1}\mathbf{Q}[\![\tilde{\mathbf{u}}]\!]\right) \tag{42}$$

Note that the product $\zeta\gamma$ is dimensionless. Making use of equations (1), (3) and (5) we obtain:

$$\mathbf{D}\boldsymbol{\varepsilon}_{\Gamma_d}^{tot}\mathbf{n} = \left(1-\omega+\zeta\gamma\omega\right)\mathbf{t}^{eff} \tag{43}$$

Under the assumption that $\boldsymbol{\varepsilon}_{\Gamma_d}^{tot}$ is kept constant during return mapping, the partial derivative of the effective traction vector with respect to damage can thus be expressed as:

$$\frac{\partial\mathbf{t}^{eff}}{\partial\omega} = \left(\frac{1-\zeta\gamma}{1-\omega+\zeta\gamma\omega}\right)\mathbf{t}^{eff} \tag{44}$$

Inserting equations (8) and (44) in (38) yields:

$$f^{j+1} = f^{j} - \left(\left(\frac{1-\zeta\gamma}{1-\omega+\zeta\gamma\omega}\right)t^{eff,eq,j} + n\left(f_t^1 - f_t^0\right)\left(\omega^j\right)^{n-1}\right)\left(\omega^{j+1}-\omega^j\right) \tag{45}$$

In the limit of $h \to 0$ we have $\zeta = \delta_{\Gamma_d}$ and (45) becomes

$$f^{j+1} = f^{j} - \left(\frac{1}{\omega^j} t^{eff,eq,j} + n\left(f_t^1 - f_t^0 \right) \left(\omega^j \right)^{n-1} \right) \left(\omega^{j+1} - \omega^j \right) \tag{46}$$

We find the updated damage variable as the root of equation (46), after setting $f^{j+1} = 0$. However, since this expression is singular for $\omega = 0$, we prefer using equation (45) with a value of $\zeta \gg 1$. This choice influences the rate of convergence of the local iterative procedure, not the global equilibrium state. ζ only appears in the return mapping scheme, not in the tangent. Therefore, selecting a high value for ζ does not render the system ill-conditioned. The updated damage variable obeys the Kuhn-Tucker conditions since $f^{j+1} = 0$ and $\Delta\omega > 0$ if $\zeta > 1$.

5 Numerical examples

In this section three different numerical examples are presented. First, a uniaxial tension test on a 3 by 3 element mesh is studied. A full parametric study of the model is performed and the simplicity of the example allows observing the influence of the individual parameters. Next, aspects of mesh objectivity are analyzed by means of a four point bending test. Finally, the applicability of the model in a multi-material setting is illustrated by means of a mode I double cantilever beam test.

5.1 Uniaxial tension

A 2D uniaxial tensile test is performed on a square sample with an edge length of 0.03 m (Figure 4). The sample is discretized with 9 square bilinear elements. Nodes on the left boundary are clamped in x-direction. Nodes at the right boundary are forced to move in x-direction at a fixed rate. Two additional constraints in y-direction prevent rigid body motions. A strong discontinuity with normal pointing in the positive x-direction is inserted in the 3 middle elements. The discontinuity is damage-free at the beginning of the computations. Plane stress conditions are assumed. The Poisson ratio is taken equal to zero to simplify interpretation of the results. The influence of changing the Young's modulus, tensile strength, residual tensile strength and hardening exponent are studied. Table 1 gives an overview of the investigated parameters. Please note that G_f^I is not an explicit model parameter, but is being calculated from equation (15).

Figure 5a shows the influence of variations in stiffness. It is observed that the stiffer the material is, the more brittle it behaves. A higher tensile strength influences the peak load, but does not affect the slope of the loading and softening branch (Figure 5b). If tensile strength and residual tensile strength are given distinct values, both slope and shape of the softening branch are altered (Figure 5c). Choosing $f_t^1 > f_t^0$ leads to a more ductile response, whereas the opposite choice, $f_t^1 < f_t^0$, results in more brittle failure or even snap-back if $f_t^1 < \left(n/(n+1) \right) f_t^0$. Snap-back could not be illustrated in Figure 5c since the test is performed under displacement control. Figure 5d illustrates the effect of the softening parameter. If $n > 1$, the slope of the softening branch becomes more convex. A more concave shape is found for $0 < n < 1$. Essential parameters E and f_t^0 can be

identified experimentally from a uni-axial tensile test. Secondary parameters f_t^1 and n require inverse analysis. Adopting different expressions for κ (instead of Eq. 8) and $\boldsymbol{\sigma}$ (instead of Eq. 18) allows describing the behavior of a wide range of materials.

5.2 Four-point bending

A four-point bending test on a notched beam is used to prove mesh objectivity of the response. The beam has a length of 0.24 m and cross-sectional dimensions 0.048 m x 0.024 m (height x depth). The notch has a width of 0.004 m, a depth of 0.008 m and a circular tip. The distance between the two supports is 0.2 m and between the loading points 0.1 m. A Young's modulus of 10 GPa, a Poisson's ratio of 0.2, a tensile strength of 3 MPa, a residual tensile strength of 2 MPa and a softening exponent of 0.6 were selected. These values are representative for meule sandstone. The simulations were performed in 2D under plane stress assumptions. Meshes were constructed for two element types (bilinear quadrilateral and linear triangle) and for three levels of mesh refinement (572, 1596 and 5604 dofs, respectively). The six meshes are depicted in Figure 6. A new crack segment is introduced at the end of a load step, if the failure criterium is violated at the crack tip. In this way, crack path continuity is easily enforced. Afterwards global equilibrium is reevaluated. The procedure is repeated until the initiation criterion is no longer met. New crack segments cross the entire element at once. Displacement control was applied.

The results of the mesh sensitivity analysis are presented in Figure 7 as 'force' versus 'opening at the notch' diagrams. Comparing the three structured meshes based on quadrilateral elements (Figure 7a) it is seen that the meshes with 1596 and 5604 dofs yield almost the same response. The mesh with 572 dofs is too coarse to capture the actual behavior.

For the meshes based on triangular elements, load drops are observed in the softening branch each time a new crack segment is introduced (Figure 7b). The presence of load drops is related to the constant strain property of the T3-element. Since we use a linear elastic constitutive relation, the stress field is constant over the element as well. Therefore, the stress field in the cohesive zone is not decaying gradually, but in a stepwise manner. Upon propagation, the stress field undergoes a stepwise change as well, and a load drop is observed. Upon mesh refinement, the number of elements over the cohesive zone increases, allowing a more accurate representation of the stress field in the cohesive zone. As a result, the number of load drops increases, but their magnitude decreases. The mesh with 5604 dofs yields the same response as the two finest meshes with quadrilateral elements.

The computations were repeated with smaller load steps. At coinciding loading points an identical response was obtained. For this example the size of the load step did not influence the robustness of the algorithm. If a nonlinear model is chosen to represent the bulk behaviour, it can be expected that there exists an upper bound to the load step.

5.3 Double cantilever beam

As a final example, a comparison between the proposed cohesive zone model and classical interface elements is presented by means of a mode I double cantilever beam test (DCB). A composite beam of 0.0025 m length and 0.0005 m height is subjected to a splitting loading (See Figure 8). The beam consists of two layers with equal height: a

softer upper layer on a stiffer base layer. Both layers have a Poisson's ratio of 0.3 and a tensile strength of 1 MPa. The stiffness of the base layer is 10 GPa. The stiffness of the upper layer is taken 5, 10, 20 and 50 times lower. The material interface is modeled in two different ways. First using the proposed cohesive zone model ($E = 10\,\text{GPa};\ \nu = 0;$ $f_t^0 = 1\,\text{MPa};\ \ f_t^1 = 1\,\text{MPa};\ \ n = 1$). This choice of parameters yields a linear softening behavior with a fracture energy of 50 N/m. Alternatively, interface elements employing a linear softening law are used. Although the use of a dummy stiffness can be avoided by e.g. initially constraining the interfaces (see [3]), we make use of classical interface elements with a dummy stiffness of 1.0E6 GPa. The tensile strength and fracture energy are taken 1 MPa and 50 N/m, respectively. The beam consists of 125 bilinear elements for the X-FEM simulation and 150 bilinear elements for the simulation with interface elements. Both meshes have 300 dofs. Plane stress conditions are assumed.

In Figure 9, the applied load F is plotted against the vertical displacement of the loading point. Dashed lines represent the solution with interface elements, solid lines are used for the X-FEM results. As expected, it is observed that the overall response is not depending on the modeling technique for the material interface. A small difference in slope of the softening branch is found with increasing difference in stiffness between the two layers. This is related to the way the equivalent traction is defined in the discrete model, namely as the normal component of the effective traction vector. In the interface element, damage evolution is governed by the norm of the displacement jump vector (normal and tangential). In the presence of shear (or a tangential jump) along the interface, damage will grow faster in the interface formulation. The importance of the shear contribution increases with increasing difference in stiffness between both layers. The good agreement between the response of the proposed cohesive zone model and of classical interface elements indicates that the introduction of the approximation for the local stress tensor at zero damage (Eq. 36) is justified.

6 Conclusions

A general strategy to model the mechanical behavior of quasi-brittle materials is proposed. The proposed discrete constitutive equation allows for a smooth transition between the continuum state and the discrete state and ensures equilibrium between the effective tractions in the undamaged material bonds and the stresses in the continuum at every stage of the failure process. The discrete equation can be used in combination with any continuum constitutive model, yielding a continuous-discontinuous material model that can describe the entire failure process. Using a linear elastic continuum model it was shown that, a mesh objective response is obtained. Besides the study of fracture processes in bulk material, the discrete model can also be applied to examine delamination or interface failure. In contrast with classical interface elements, no dummy stiffness is required.

The predictive capabilities of the model crucially depend on the characteristics of the continuum model and the appropriate choice of the damage criterion. It was shown that for mode I, realistic results and trends can already be obtained based on a simple mechanical model (linear elasticity) and failure criterion (Rankine). Extension to other models and failure criteria can be done in an analogue way.

7 Acknowledgements

Funding for this work was provided by the Flemish institute for Science and Technology (IWT-SBO project IT300175).

8 References

[1] G.I. Barenblatt, *The mathematical theory of equilibrium cracks in brittle fracture*, Advances in applied mechanics 7 (1962) p. 55-129.

[2] T. Belytschko and T. Black, *Elastic crack growth in finite elements with minimal remeshing*, Internat. J. Numer. Methods Engrg. 45 (1999) p. 601-620.

[3] G.T. Camacho and M. Ortiz, *Computational modeling of impact damage in brittle materials*, Internat. J. Solids Structures 33 (1996) p. 2899-2938.

[4] J. Dolbow, N. Moës and T. Belytschko, *Discontinuous enrichment in finite elements with a partition of unity method*, Finite Elem. Anal. Des. 36 (2000) p. 235-260.

[5] C.A. Duarte and J.T. Oden, *H-p clouds - an h-p meshless method*, Numer. Methods Partial Differential Equations 12 (1996) p. 673-705.

[6] D.S. Dugdale, *Yielding of steel sheets containing slits*, J. Mech. Phys. Solids 8 (1960) p. 100-104.

[7] M. Jirásek, *Embedded crack models for concrete fracture*, in *EURO-C 1998 Computer modeling of concrete structures*, R. de Borst, N. Bicanic, H. Mang and G. Meschke, eds., Balkema, Rotterdam, 1998.

[8] M. Jirásek and T. Zimmermann, *Embedded crack model. Part II: Combination with smeared cracks*, Internat. J. Numer. Methods Engrg. 50 (2001) p. 1291-1305.

[9] J. Lemaitre, *A continuous damage mechanics model for ductile fracture*, J. Engrg. Mater. and Technol. 107 (1985) p. 83-87.

[10] N. Moës, J. Dolbow and T. Belytschko, *A finite element method for crack growth without remeshing*, Internat. J. Numer. Methods Engrg. 46 (1999) p. 131-150.

[11] J. Oliver, *On the discrete constitutive models induced by strong discontinuity kinematics and continuum constitutive equations*, Internat. J. Solids Structures 37 (2000) p. 7207-7229.

[12] J. Oliver, A.E. Huespe, M.D.G. Pulido and E. Chaves, *From continuum mechanics to fracture mechanics: the strong discontinuity approach*, Engrg. Fracture Mech. 69 (2002) p. 113-136.

[13] K.D. Papoulia, C.-H. Sam and S.A. Vavasis, *Time continuity in cohesive finite element modeling*, Internat. J. Numer. Methods Engrg. 58 (2003) p. 679-701.

[14] Z. Ren and N. Bićanić, *Simulation of progressive fracturing under dynamic loading conditions*, Comm. Numer. Methods Engrg. 13 (1997) p. 127-138.

[15] J.C. Simo and J.W. Ju, *Strain- and stress-based continuum damage models – 1. Formulation*, Internat. J. Solids Structures 23 (1987) 821-840.

[16] A. Simone, G.N. Wells and L.J. Sluys, *From continuous to discontinuous failure in a gradient-enhanced continuum damage model*, Comput. Methods Appl. Mech. Engrg. 192 (2003) p. 4581-4607.

[17] G.N. Wells and L.J. Sluys, *A new method for modelling cohesive cracks using finite elements*, Internat. J. Numer. Methods Engrg. 50 (2001) p. 2667-2682.

	E [GPa]	f_t^0 [MPa]	f_t^1 [MPa]	n [-]	G_f^I [N/m]
(a)	**2.0**	3.0	3.0	1.0	2250.0
	5.0	3.0	3.0	1.0	900.0
	10.0	3.0	3.0	1.0	450.0
	20.0	3.0	3.0	1.0	225.0
	50.0	3.0	3.0	1.0	90.0
(b)	10.0	**2.0**	2.0	1.0	200.0
	10.0	**2.5**	2.5	1.0	312.5
	10.0	**3.0**	3.0	1.0	450.0
	10.0	**3.5**	3.5	1.0	612.5
	10.0	**4.0**	4.0	1.0	800.0
(c)	10.0	3.0	**1.5**	1.0	262.5
	10.0	3.0	**3.0**	1.0	450.0
	10.0	3.0	**4.5**	1.0	712.5
	10.0	3.0	**6.0**	1.0	1050.0
	10.0	3.0	**7.5**	1.0	1462.5
(d)	10.0	3.0	4.5	**0.2**	905.4
	10.0	3.0	4.5	**0.5**	806.3
	10.0	3.0	4.5	**1.0**	712.5
	10.0	3.0	4.5	**2.0**	622.5
	10.0	3.0	4.5	**5.0**	535.2

Table 1: Investigated parameter combinations and resulting fracture energy (according to Eq. 15) for the uniaxial tensile test. Tests are subdivided in four groups (a-d). Corresponding results are shown in Figure 5a-d.

FIGURE CAPTIONS

Figure 1: Schematic representation of (a) an infinitesimal part of a plane with normal **n** in a structure or structural component, (b) the cohesive zone with approximately 60% in-plane micro-damage and (c) the relation between damage, effective tractions and continuum stresses.

Figure 2: Schematic representation of (a) the components of the traction vector as a function of damage and (b) displacement jump. Tractions are indicated with a solid line, effective tractions with a dotted line and the continuum part of the traction with a dashed line.

Figure 3: (a) Body Ω crossed by a displacement discontinuity. (b) Schematic representation of the displacement field and (c) the corresponding strain field of a crossed 1D element.

Figure 4: Uniaxial tensile test: geometry, mesh and boundary conditions.

Figure 5: Uniaxial tensile test: sensitivity analysis of (a) Youngs modulus, (b) tensile strength, (c) residual tensile strength and (d) hardening exponent. All parameter combinations are listed in **Error! Reference source not found.**.

Figure 6: 4pt-bending test: geometry, meshes and boundary conditions.

Figure 7: 4pt-bending test: load-displacement curves obtained with meshes based on (a) Q4 and (b) T3 elements.

Figure 8: Double cantilever beam: geometry, mesh and boundary conditions.

Figure 9: Double cantilever beam: load-displacement curves for various material combinations as obtained with the cohesive zone model (solid line) and interface elements (dashed line).

FIGURE 1

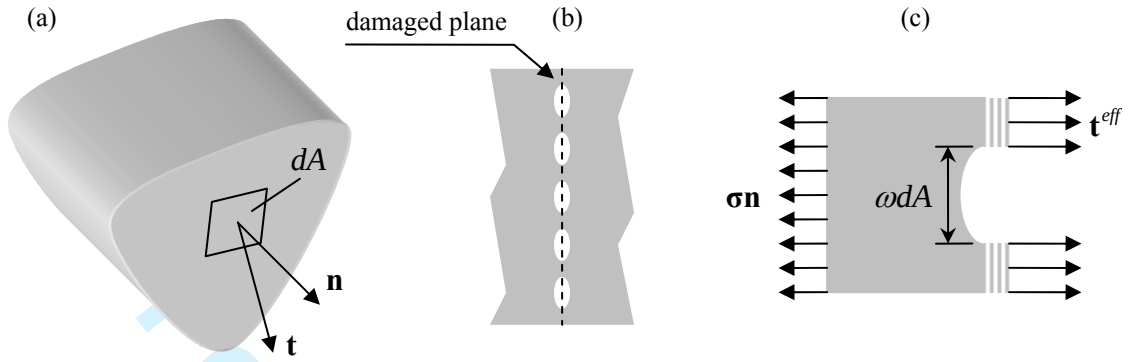

FIGURE 2

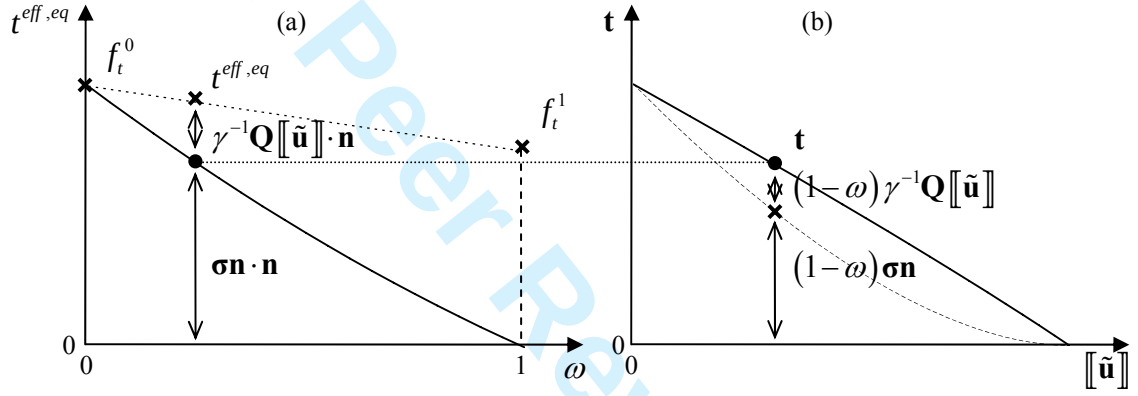

FIGURE 3

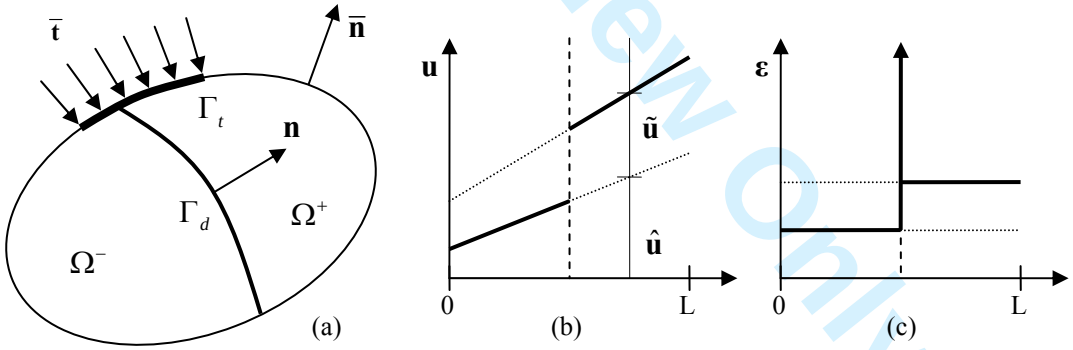

FIGURE 4

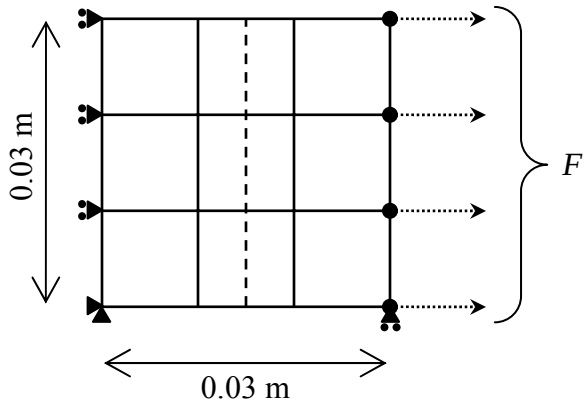

FIGURE 5

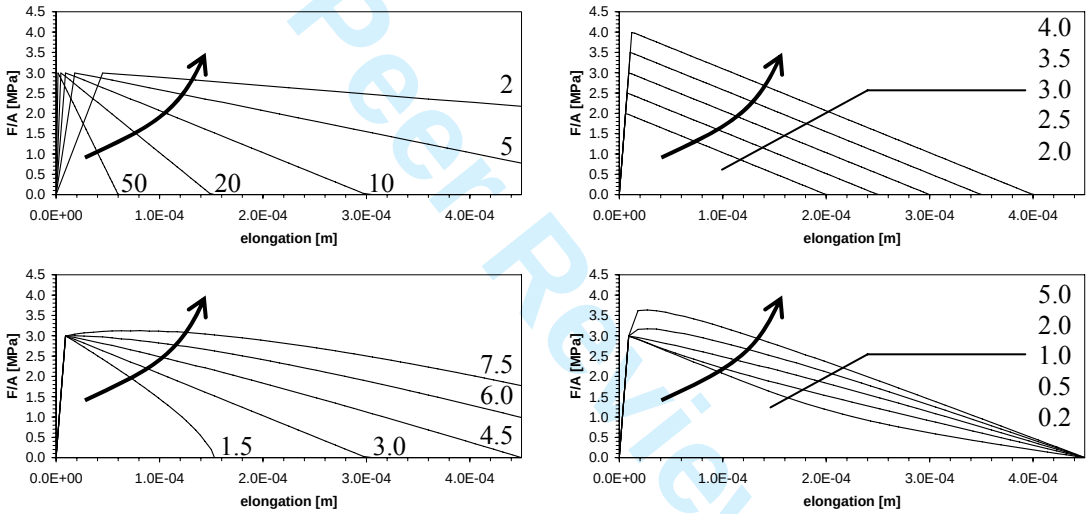

FIGURE 6

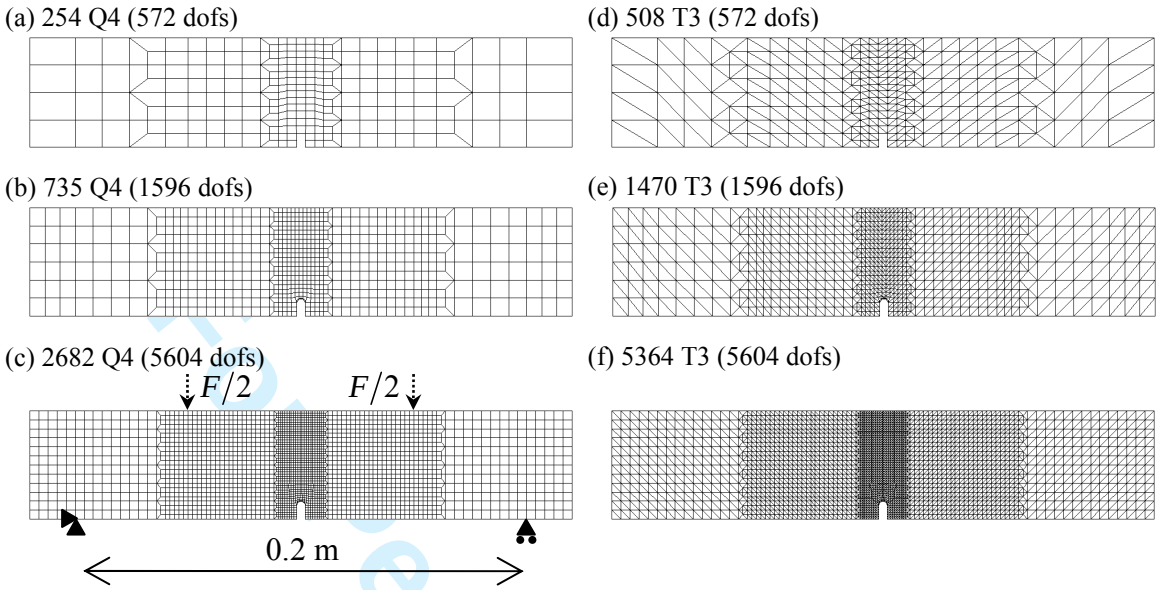

FIGURE 7

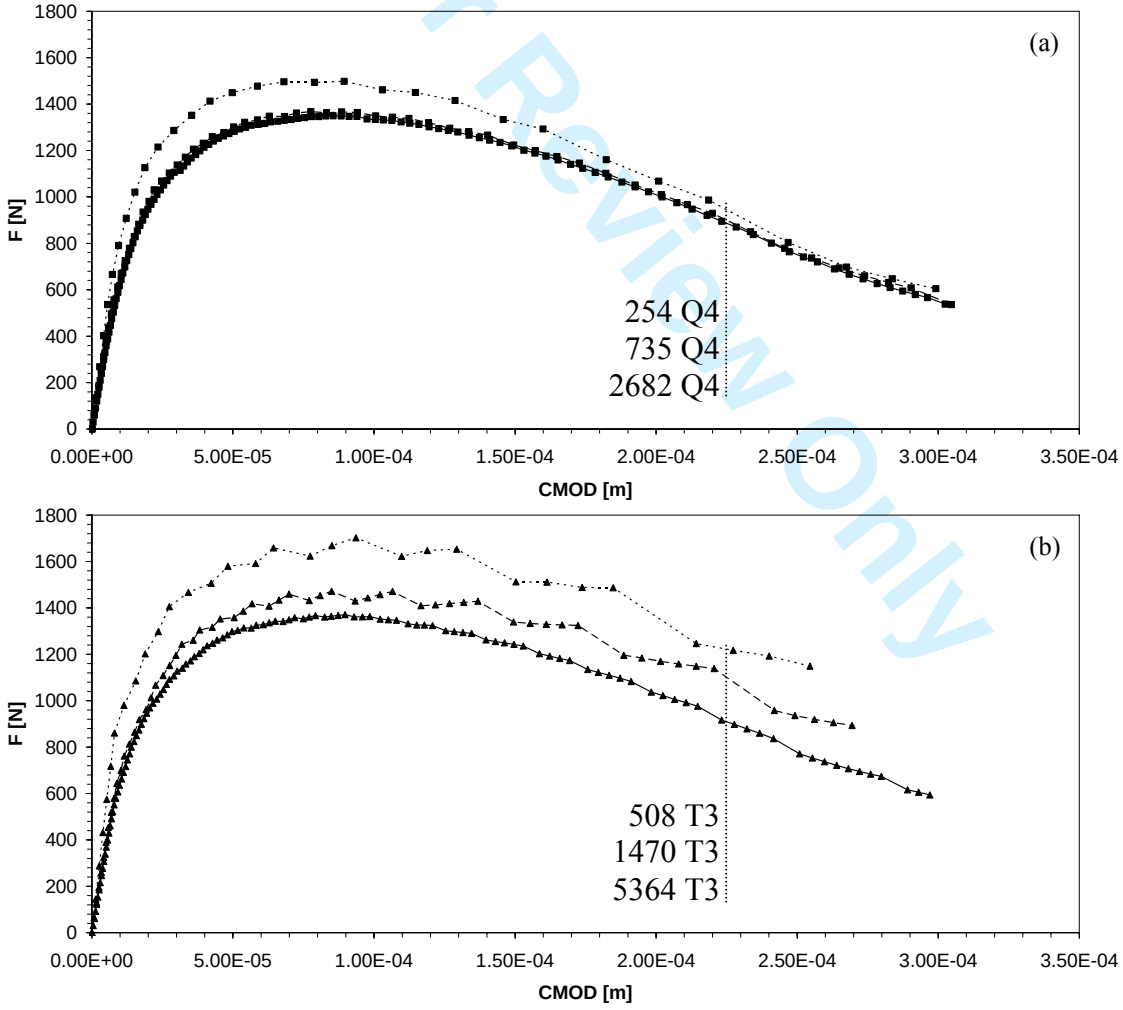

FIGURE 8

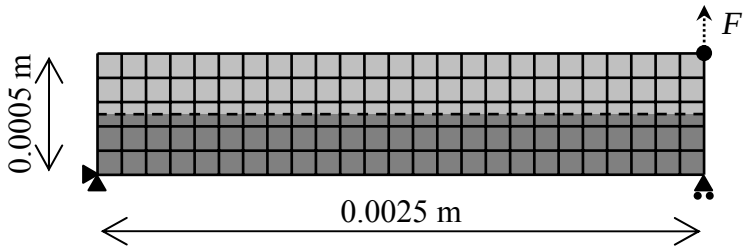

FIGURE 9